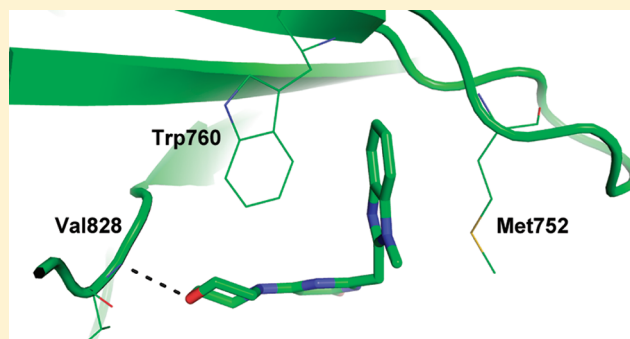


Discovery and Optimization of New Benzimidazole- and Benzoxazole-Pyrimidone Selective PI3K β Inhibitors for the Treatment of Phosphatase and TENsin homologue (PTEN)-Deficient Cancers

Victor Certal,[†] Frank Halley,^{*,†} Angela Virone-Oddos,[†] Cécile Delorme,[†] Andreas Karlsson,[‡] Alexey Rak,[‡] Fabienne Thompson,[†] Bruno Filoche-Rommé,[†] Youssef El-Ahmad,[†] Jean-Christophe Carry,[†] Pierre-Yves Abecassis,[§] Pascale Lejeune,[†] Loic Vincent,[†] Hélène Bonnevaux,[†] Jean-Paul Nicolas,[†] Thomas Bertrand,[‡] Jean-Pierre Marquette,[‡] Nadine Michot,^{||} Tsiala Benard,[⊥] Peter Below,[#] Isabelle Vade,[†] Fabienne Chatreaux,[†] Gilles Lebourg,[†] Fabienne Pilorge,[†] Odile Angouillant-Boniface,[†] Audrey Louboutin,[†] Christoph Lengauer,[†] and Laurent Schio[†]

[†]Oncology Drug Discovery, [‡]Structural Biology and Molecular Modeling, [§]Drug Safety, ^{||}Protein Production, [⊥]Formulation, [#]Parallel Synthesis, Sanofi Research & Development, 13 quai Jules Guesde, 94403 Vitry-sur-Seine, France

ABSTRACT: Most of the phosphoinositide-3 kinase (PI3K) kinase inhibitors currently in clinical trials for cancer treatment exhibit pan PI3K isoform profiles. Single PI3K isoforms differentially control tumorigenesis, and PI3K β has emerged as the isoform involved in the tumorigenicity of PTEN-deficient tumors. Herein we describe the discovery and optimization of a new series of benzimidazole- and benzoxazole-pyrimidones as small molecular mass PI3K β -selective inhibitors. Starting with compound **5** obtained from a one-pot reaction via a novel intermediate **1**, medicinal chemistry optimization led to the discovery of compound **8**, which showed a significant activity and selectivity for PI3K β and adequate in vitro pharmacokinetic properties. The X-ray costructure of compound **8** in PI3K δ showed key interactions and structural features supporting the observed PI3K β isoform selectivity. Compound **8** achieved sustained target modulation and tumor growth delay at well tolerated doses when administered orally to SCID mice implanted with PTEN-deficient human tumor xenografts.



INTRODUCTION

Phosphoinositide 3-kinase (PI3K) pathway activation plays a major role in cancer as a result of abnormalities in major components of this signaling cascade, including activating point mutations and/or amplification of the *PIK3CA* gene as well as loss of negative regulatory proteins such as Phosphatase and TENsin homologue (PTEN).¹ In addition, aberrant signaling through this pathway has been shown to represent a key mechanism of resistance to anticancer therapies including targeted therapy. PI3K is considered as one of the most promising target in this pathway for cancer treatment. Class I PI3Ks are lipid kinases comprising four isoforms, PI3K α , PI3K β , PI3K δ , and PI3K γ , that generate phosphatidylinositol 3,4,5-triphosphate (PIP3), a second messenger involved in Akt activation. Cellular PIP3 levels are tightly regulated by PTEN lipid phosphatase, which converts PIP3 into phosphatidylinositol 4,5-bisphosphate (PIP2). The class I PI3Ks is further divided into class IA comprising PI3K α , PI3K β and PI3K δ , which are activated by receptor tyrosine kinases or GPCR (PI3K β) and subclass IB with a single member, PI3K γ , activated by GPCRs. Class IA proteins which consist of a catalytic subunit (p110 α , p110 β , p110 δ) and a regulatory

subunit represent the only enzymes clearly implicated in human cancer.^{1,2} Most of the PI3K inhibitors currently in clinical development are pan-PI3K inhibiting all four class I PI3K isoforms. However, recent reports support the clinical development of isoform-specific inhibitors.^{3,4} Indeed, first clinical trials with pan-PI3K inhibitors performed on nonstratified cancer patient cohorts appear to be less successful than expected, with no clear genetic determinant of sensitivity observed yet. On the basis of preclinical studies, while PI3K α -specific inhibition is predicted to block the growth of tumors harboring *PIK3CA* mutations, PTEN-deficient tumors have been shown to depend on PI3K β activity. Indeed, it has been reported that conditional knockout of *PIK3CB*, and not *PIK3CA*, leads to tumor growth inhibition in PTEN-deficient genetic context, as well as to prevent prostate tumor formation induced by *PTEN* loss with concomitant diminution of AKT phosphorylation.^{5,6} Selective compounds against PI3K α or PI3K β isoforms could be developed on stratified cancer patient subpopulations based on *PIK3CA* mutant or *PTEN* deficient genotypes, respectively.

Received: February 23, 2012

Published: April 23, 2012

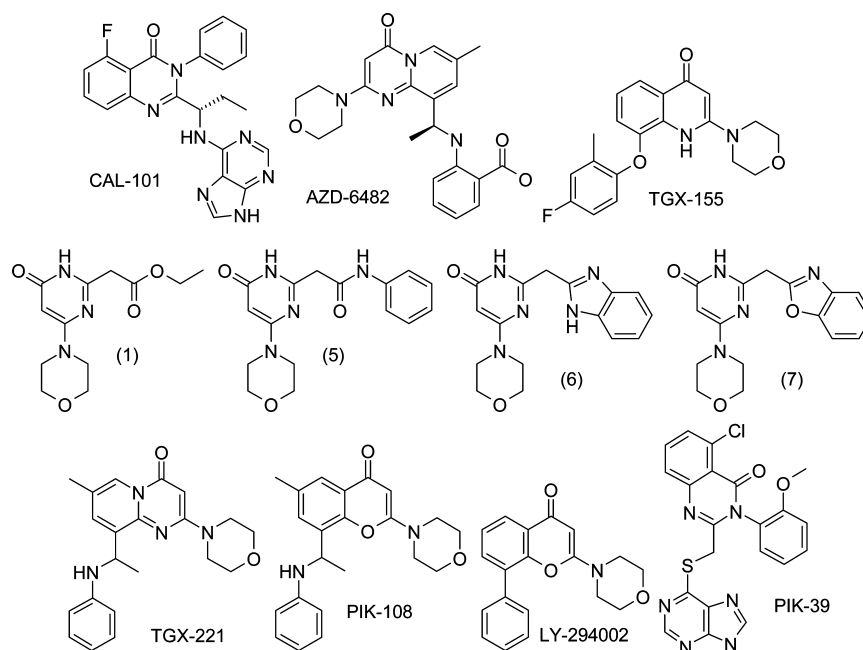


Figure 1. Structure of some PI3K inhibitors.

Furthermore, isoform-specific PI3K inhibitors may exhibit better therapeutic windows compared to pan-PI3K inhibitors and, depending on their pharmacological properties, could be favorably combined with other targeted therapies or standard of care agents.

Until very recently, relatively few isoform-selective PI3K inhibitors, exhibiting appropriate drug-like properties, have been described. CAL-101 was the first isoform-selective compound entering clinical trials for the treatment of cancer. On the basis of the restricted expression of PI3K δ isoform in hematopoietic cells, this PI3K δ -selective compound is currently being developed in hematologic cancer malignancies.^{7,8} phase 1 clinical trials with the PI3K β -selective inhibitors, AZD-6482 and TGX-155, were performed some years ago for thrombosis but to the best of our knowledge these compounds were never developed for cancer treatment. Very recently, PI3K α -selective inhibitors have entered clinical phase 1 for *PIK3CA* mutated cancer patients.^{9,10} As part of our ongoing drug discovery and development activities for targeted cancer therapies, we have initiated the search for PI3K isoform-selective inhibitors. We had previously reported the identification of PI3K α /mTOR and PI3K α modulators that demonstrated some level of antiproliferative selectivity in *PIK3CA* mutant versus PTEN-deficient cancer cells.¹¹ Similarly, we have also described PI3K β -selective kinase inhibitors exhibiting superior cellular activity in PTEN-deficient versus *PIK3CA* mutant tumor cells.¹²

We report herein the discovery and optimization of a novel series of PI3K β isoform-selective small molecular mass inhibitors and their potential application as anticancer agents in PTEN-deficient tumor models.

LEAD DISCOVERY AND OPTIMIZATION

Starting from a high-throughput screening campaign and following early hit validation and chemical exploration, we identified compound **5**^{13,14} (Figure 1), which presented some interesting selectivity for PI3K β versus other PI3K isoforms (IC₅₀ = 2133 nM, 42 nM, 118 nM, and >10 μ M on PI3K α , β , δ ,

and γ , respectively) in biochemical assays. Subsequent medicinal chemistry efforts were devoted to the replacement of the potentially labile anilide moiety to bioisosteric benzimidazole or benzoxazole analogues. The unsubstituted benzimidazole compound **6**¹⁵ (IC₅₀ >10 μ M, 158 nM, 2870 nM, and >10 μ M on PI3K α , β , δ , and γ , respectively) and benzoxazole compound **7**¹⁵ (IC₅₀ >10 μ M, 82 nM, 779 nM, and >10 μ M on PI3K α , β , δ , and γ , respectively) displayed a remarkable level of PI3K β selectivity while maintaining high ligand efficiency (LE) values¹⁶ of 0.40 and 0.42, respectively.

At the time we initiated this work, PI3K β specific inhibitors derived from different chemotypes such as the quinolone TGX-155,¹⁷ pyridopyrimidone TGX-221,¹⁸ and chromenone PIK-108¹⁸ were reported in several publications. However, structural information on their binding modes was limited and only an X-ray structure of the closely related pan-PI3K modulator LY-294002 in complex with PI3K γ was available.¹⁹ To determine the binding mode of the pyrimidone benzimidazoles, we attempted cocrystallization in the surrogate enzyme PI3K γ , but all efforts failed, probably due to their poor PI3K γ binding affinity (IC₅₀ > 10 μ M). To overcome this limitation, we decided to embark on the thorough exploration of the structure–activity relationship (SAR) of this series, introducing additional substituents to improve biological activity and drug-like properties.

To guide compound potency and selectivity improvement on PI3K β , we generated a homology model of PI3K β based on ligand-bound PI3K γ X-ray structures available in-house and in the public domain (PDB).^{19,20} Interestingly, the homology model that best accommodated the compounds allowed the identification of a region in the P-loop, made accessible by movement of a conserved methionine (Met779), previously described as the selectivity pocket (Met804 in PI3K γ).²⁰ In our model, the docked compounds adopt a nonplanar geometry where the morpholine makes a hydrogen bond with the hinge backbone NH of Val854. The pyrimidone scaffold occupies the central part of the ATP binding site from where the benzimidazole side chain is projected into the selectivity pocket

where it is stacking against the side chain of Trp787. Given strong analogies with, on the one hand the morpholine containing ligands, and on the other hand the “propeller shaped”²⁰ inhibitors such as PIK-39 (Figure 1), we confidently adopted this binding mode hypothesis for analyzing SAR and drive optimization of the pyrimidone series potency (see Figure 2).

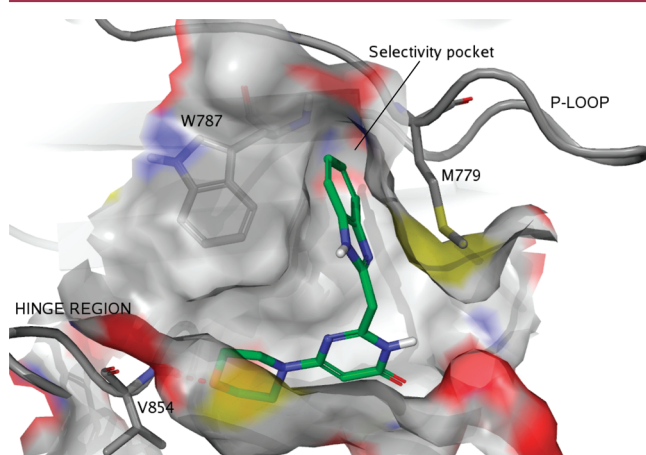


Figure 2. Proposed binding mode of pyrimidone benzimidazoles in PI3K β showing favorable interactions with the hinge region (V854) and the selectivity pocket (M779).

During this process, we examined the activity of these compounds on the four PI3K isoforms in biochemical assays and target modulation in tumor cells. To further confirm their selectivity profile against other members of the lipid kinase family, the new compounds were evaluated for mTOR inhibition and shown to be all inactive ($IC_{50s} > 10 \mu M$) in a biochemical assay. Target modulation in tumor cells was assessed by measuring the inhibition of Akt phosphorylation in the PTEN-deficient PC3 prostate cancer cell line. We first demonstrated for a set of molecules, including reference compounds, that PI3K β -selective compounds inhibited Akt phosphorylation at both T308 (phosphorylated by PDK1 kinase)²¹ and S473 (phosphorylated by mTORC2 kinase)²¹ residues with the same level of activity. As exemplified in Table 1, reference compounds and pyrimidone benzimidazoles exhibited roughly the same potency on pAkt (T308) and

Table 1. Cellular Activity of Reference Compounds and Pyrimidone Benzimidazoles on Akt Phosphorylation at T308 and S473 Residues in PC3 Cell Line

compd	biochemical activity PI3K β ^a IC_{50} (nM)	cellular activity		
		pAkt ^a (T308) IC_{50} (nM)	pAkt ^a (S473) IC_{50} (nM)	IC_{50} ratio pAkt (T308)/(S473)
TGX-221	30	3	10	0.30
PIK-108	28	3	3	1.00
8	99	188	76	2.47
9	30	100	41	2.44

^a IC_{50} values are reported as the mean from at least two independent experiments; see Experimental Methods for assay details.

pAkt (S473), the ratio of IC_{50} (T308)/(S473) varying from 0.3 to 2.5, which stands within assay variability.

Consequently, in the following Tables 2–5, we only report pAkt (S473) inhibition in cells to document pharmacodynamic modulation of the PI3K pathway.

The optimization of the benzimidazole (see Table 2) and benzoxazole (see Table 3) series was performed in parallel to exploit potential differences in the physicochemical properties between these two structurally distinct chemotypes.

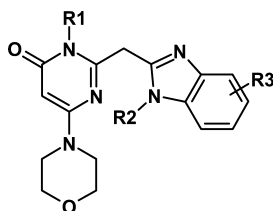
Analysis of the data presented in Table 2 showed that introduction of a halogen (compounds 9, 13, and 14) brought the level of inhibitory activity below 100 nM. Introduction of the *N*-methyl benzimidazole compound 8 also led to a slight improvement of activity, comparable to the combination of 5-fluoro and *N*-methyl benzimidazole as in compound 11, however, the 6-fluoro isomer 12 was less potent. Adding a methyl group on the *N*-H of the pyrimidone scaffold as in compound 10 led to a 15-fold loss in activity. This drastic drop in potency suggested that polar groups interacting with the residues Asp937 or Lys805 in PI3K β would be preferred at this position. Contrary to the effect observed with halogens, introduction of a methyl, an electron donating methoxy or an electron withdrawing trifluoromethyl (compounds 15–17), did not enhance activity. Substitution of the benzimidazole nitrogen with groups larger than methyl such as ethyl, cyclopropyl, methoxyethyl, cyclohexyl, phenyl, or benzyl (compounds 18–23) led to some activity modulation albeit with a loss of selectivity over PI3K δ , especially for compounds 21–23, which were even more potent on PI3K δ . Introduction of the 4-phenyl (compound 24) led to a binding activity increase of over 10-fold with PI3K β $IC_{50} = 10nM$, however, with a similar selectivity over PI3K δ . The *N*-methyl 4-phenyl compound 25 and the *N*-methyl 7-phenyl compound 26 were both equally potent, suggesting that there is room for the *N*-methyl group to adopt both the inward and outward positions in the selectivity pocket. The proposed binding mode was also in agreement with the loss of activity observed with the 5-phenyl and the 6-phenyl (compounds 27–28) because in these positions the phenyl group would clash with residues in the P-loop.

Overall, we globally observed a relatively good relation between the biochemical activity values and cellular potency for the benzimidazole derivatives reported in Table 2. It is interesting to point out that when plotting cellular potency against biochemical activity on PI3K β , a trend for correlation ($r^2 = 0.45$, see Figure 3) was observed, suggesting an overall modest cellular permeability. When removing the benzimidazole *N*-H compounds from this set, the correlation went up to $r^2 = 0.67$.

In the benzoxazole series (see Table 3), a fluorine scan (29–32) showed only a modest (2-fold) increase in potency for the 5-fluoro derivative compound 30.

Similar results were obtained in a methyl scan (compounds 33–37). In this case, a >10-fold drop in activity was observed for the *N*-methyl pyrimidone derivative 33, which is consistent with the data obtained with compound 10 in the benzimidazole series. The synthetic intermediate 4-bromo 38 showed activity comparable to the 4-fluoro 29 and the 4-methyl 34. The 4-phenyl 39 showed a 4-fold increase in potency over the 7-phenyl 40, and although there is no steric difference between the two compounds, one possible explanation might lay in the observation that Met779 is facing the azole part of the ligand via its sulfur atom in a configuration stabilizing a *N*...S

Table 2. Biochemical and Cellular Activity of Pyrimidone Benzimidazoles (6, 8–26) and Reference Compounds (TGX-221, TGX-155, and PIK-108)



compd	R1	R2	R3	MW	PI3K α^a IC ₅₀ (nM)	PI3K β^a IC ₅₀ (nM)	PI3K δ^a IC ₅₀ (nM)	PI3K γ^a IC ₅₀ (nM)	pAkt ^a (S473) IC ₅₀ (nM)
TGX-221				364	>10000	30	851	>10000	10
TGX-155				354	>10000	32	166	>10000	72
PIK-108				364	>10000	28	658	>10000	3
6	H	H	H	311	>10000	158	2870	>10000	665
8	H	Me	H	325	>10000	99	1395	>10000	76
9	H	H	5-F	329	>10000	30	219	>10000	41
10	Me	H	5-F	343	>10000	739	5715	>10000	
11	H	Me	5-F	343	>10000	82	855	>10000	16
12	H	Me	6-F	343	>10000	290	1060	>10000	289
13	H	H	5-Br	390	5460	91	442	>10000	85
14	H	H	5-Cl	346	5650	99	247	>10000	63
15	H	H	5-Me	325	9880	450	2210	>10000	140
16	H	H	5-OMe	341	>10000	193	397	>10000	475
17	H	H	5-CF ₃	379	>10000	386	2850	>10000	961
18	H	Et	H	339	1000	72	225	8270	26
19	H	cyclopropyl	5-F	369	>10000	29	36	>10000	9
20	H	-EtOMe	H	387	>10000	205	270	>10000	109
21	H	cyclohexyl	H	393	8400	90	21	>10000	142
22	H	Ph	H	387	6790	75	36	>10000	8
23	H	-CH ₂ Ph	H	401	5725	111	84	>10000	105
24	H	H	4-Ph	387	5503	10	180	>10000	65
25	H	Me	4-Ph	401	314	57	274	>10000	26
26	H	Me	7-Ph	401	4575	60	181	>10000	17
27	H	Me	5-Ph	401	>10000	>10000	6748	>10000	
28	H	Me	6-Ph	401	7798	3410	3406	>10000	

^aIC₅₀ values are reported as the mean from at least two independent experiments; see Experimental Methods for assay details.

nonbonded interaction between the C–S–C fragment and the benzimidazole ring.²² Indeed, when searching the PDB (Protein Data Bank) with the IsoStar knowledge base²³ (version 2.1.2 tool package from CSD-Cambridge Structural Database), 483 interactions between the methylthio moiety of a methionine and an aromatic or sp² N were found compared to eight interactions with an aromatic oxygen (although this search did not take into account the methionine orientation). Replacement of the 4-phenyl with the 4-thien-2-yl **41** or a 4-pyridyl (**42–44**) did not lead to an improvement of affinity. The best activity was obtained with the 4-phenyl-5-fluoro derivative **45**, which reached the single-digit nanomolar IC₅₀ value in both biochemical and cellular assays, showing again the beneficial effect of the 5-fluorine. When plotting the cellular pAkt values against the biochemical activities on PI3K β , for the benzoxazole series, we obtained a better correlation ($r^2 = 0.801$, see Figure 4) than the one observed for the benzimidazole series, suggesting in particular a superior overall cell penetration.

The SAR generated for the benzimidazole and benzoxazole series indicate that R1 substitution with methyl leads to impairment of activity, while large groups such as phenyl at positions 4 or 7 or halogens (fluorine) at position 5 provide favorable interactions.

Potent benzimidazole and benzoxazole derivatives (PI3K β IC₅₀ < 100 nM and pAkt < 500 nM) were further evaluated for thermodynamic solubility at pH 7.4²⁴ and in vitro pharmacokinetic properties including intestinal permeability, microsomal stability, and CYP3A4 inhibition (see results in Table 4). All selected compounds have molecular weight below 450 and ClogP below 4.2, and none has any significant inhibitory activity on recombinant human CYP3A4 (IC₅₀ > 40 μ M except for compound **41** = 19 μ M).

Aqueous solubility on the other hand was surprisingly low, considering the low molecular weight and low ClogP of these compounds. We suspected strong crystal packing with intermolecular hydrogen bonding and hydrophobic interactions, especially for compounds **11**, **13**, **14**, **24**, **26**, **30**, **39**, **40**, **41**, and **45** that have thermodynamic solubility less than 50 μ M. Melting points measured for some compounds were indeed found to be high (>260 °C), which is in agreement with a strong crystal packing. Permeability measurements in CaCo2 cell lines TC7 clone²⁵ were found to be variable for benzimidazoles and high for benzoxazoles, without any correlation ($r^2 = 0.146$) with polar surface area (PSA). We found that all N–H benzimidazoles (R2=H) **9**, **13**, **14**, and **24** had low permeability (<20 nm/s), and almost all N-substituted benzimidazoles had better permeability except for **18** and **21**,

Table 3. Biochemical and Cellular Activity of Pyrimidone Benzoxazoles (7, 29–45) Substitution

compd	R1	R2	MW	PI3K α^a IC ₅₀ (nM)	PI3K β^a IC ₅₀ (nM)	PI3K δ^a IC ₅₀ (nM)	PI3K γ^a IC ₅₀ (nM)	pAkt a IC ₅₀ (nM)
7	H	H	312	>10000	82	779	>10000	62
29	H	4-F	330	>10000	567	8450	>10000	125
30	H	5-F	330	>10000	46	854	>10000	26
31	H	6-F	330	>10000	126	9040	>10000	49
32	H	7-F	330	>10000	373	2555	>10000	88
33	Me	H	326	>10000	1333			
34	H	4-Me	326	>10000	461	2755	3333	75
35	H	5-Me	326	>10000	960			233
36	H	6-Me	326	9768	526	1137	>10000	143
37	H	7-Me	326	7150	425	2385	>10000	202
38	H	4-Br	391	>10000	585	2271	>10000	127
39	H	4-Ph	388	7754	19	373	>10000	13
40	H	7-Ph	388	>10000	90	1181	>10000	177
41	H	4-thiophen-2-yl	394	4357	46	398	5742	22
42	H	4-pyridin-2-yl	389	3333	336	2170	>10000	113
43	H	4-pyridin-3-yl	389	>10000	156	335	>10000	44
44	H	4-pyridin-4-yl	389	>10000	158	995	>10000	47
45	H	4-Ph; 5-F	406	>10000	8	151	>10000	6

^aIC₅₀ values are reported as the mean from at least 2 independent experiment; see Experimental Methods for assay details.

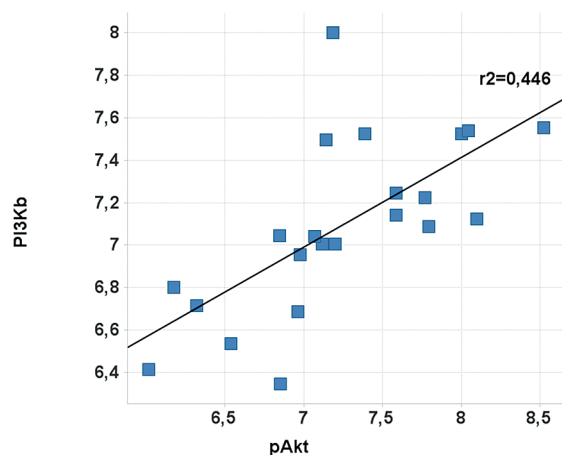


Figure 3. PI3K β biochemistry pIC₅₀ and pAkt cellular pIC₅₀ correlation for the benzimidazoles 6–9 and 11–26.

R2=Et and cyclohexyl, respectively. To elucidate the low permeability of the benzimidazoles, we assessed transport in both apical to basolateral (A–B) and basolateral to apical (B–A) directions across the cell monolayer, enabling the efflux ratio determination which was found to be high (>10). Benzoxazoles, on the other hand, displayed lower efflux ratio (<5). Overall, we could observe that low permeability was linked to strong efflux ratio, most likely due to P-gp interaction. Metabolic lability measurements were found to be high (>40%) for all compounds except 8, 11, and 45 in human liver microsomes and also for half of the compounds (18, 19, 21, 22, 24–26, 40, and 41) in mouse liver microsomes. As illustrated in the heat map (Figure 5), compound 8 was the only molecule with a well balanced in vitro pharmacological

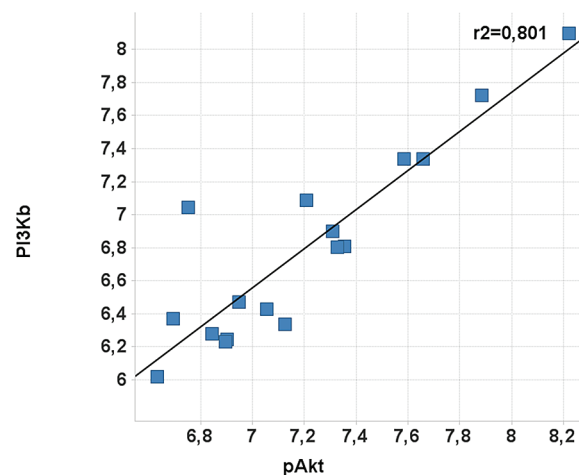


Figure 4. PI3K β biochemistry pIC₅₀ and pAkt cellular pIC₅₀ correlation for the benzoxazoles 7–32 and 34–45.

profile and was thus selected for further structural and biological characterization.

The protein kinase selectivity for this compound was assessed with a Caliper-based assay²⁶ on a 192-kinases panel. Remarkably, the compound was found highly selective with no activity up to 10 μ M on all kinases tested, including mTOR (data not shown).

X-Ray Structure of Compound 8 in PI3K δ . At the time of this work, PI3K γ was the only PI3K isoform for which X-ray structures of protein–ligand complexes could be readily obtained. However, despite numerous attempts, no ligand–protein complex structures were successfully obtained with the pyrimidone benzimidazole series in PI3K γ , probably due to its

Table 4. In Vitro and Calculated Properties of Active Compounds 7–9, 11, 13, 14, 18, 19, 21, 24–26, 30, 39–41, and 45

compd	MW	PI3K β^a IC ₅₀ (nM)	pAkt ^a (S473) IC ₅₀ (nM)	ClogP	PSA	solubility pH 7.4 μ M	CaCo2 Papp (nm/s)	MLM ^b % lability	HLM ^c % lability	rhCYP3A4 ^d IC ₅₀ μ M
7	312	82	62	1.8	80	160	199	7	41	>40
8	325	76	130	2	72	65	30	13	27	>40
9	329	30	41	1.7	83	76	2	0	69	>40
11	343	82	150	2	72	3	31	20	39	>40
13	390	91	85	2.4	83	3	0	27	75	>40
14	346	99	63	1.9	83	3	0	35	78	>40
18	339	72	26	2.5	72	221	5	48	60	>40
19	369	29	9	2.4	72		22	99	99	>40
21	393	90	142	4.1	72		15	96	97	>40
22	387	75	8	3.9	72	397	44	100	98	>40
24	387	10	65	3.2	83	3	1	51	78	>40
25	401	57	26	3.8	72		114	40	41	>40
26	401	60	17	3.8	72	2	39	55	57	>40
30	330	46	26	1.9	80	3	160	23	47	>40
39	388	19	13	3.6	80	3	310	26	40	>40
40	388	90	177	3.6	80	3	323	61	57	>40
41	432	46	22	3.4	108	3	255	79	60	19
45	406	8	6	4.1	80	15	371	17	18	>40

^aIC₅₀ values are reported as the mean from at least 2 independent experiments, see Experimental Methods for assay details. ^bMouse liver microsomes. ^cHuman liver microsomes. ^dRecombinant human CYP3A4.

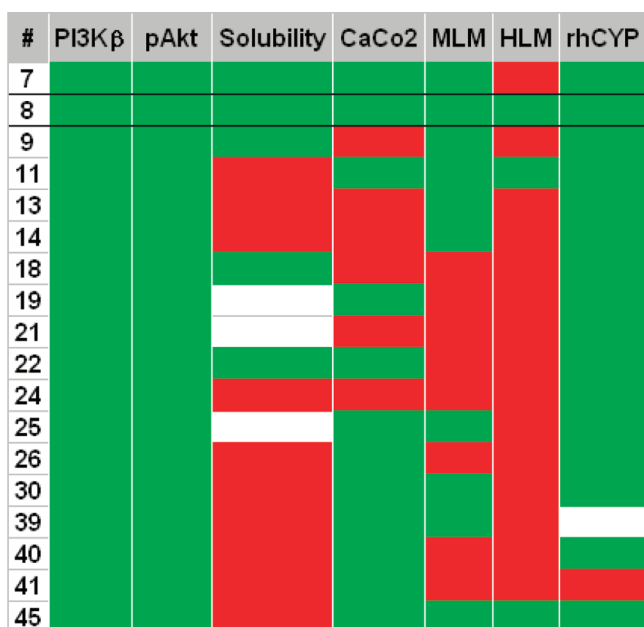


Figure 5. Heat map of Table 4 properties with selected thresholds (with the color coding: green, pass; red, fail).

limited affinity for this isoform. Recently, the X-ray structure of PI3K δ was described in its apo-form as well as in complex with ligands displaying diverse selectivity profiles, including compounds with PI3K β inhibition.²⁷ To compensate the lack of a PI3K β X-ray structure, and encouraged by measurable potency of our compounds on the PI3K δ isoform, we set about to solve the structure of PI3K δ in complex with the pyrimidone series. The structure of compound 8 (IC₅₀ of 1395 nM on PI3K δ) was solved in PI3K δ (Figure 6), revealing a binding mode in agreement with the binding mode hypothesis in PI3K β used for pyrimidone benzimidazole optimization. The morpholine moiety bound the hinge region via the main-chain nitrogen of Val828 in a very similar manner to what had been described

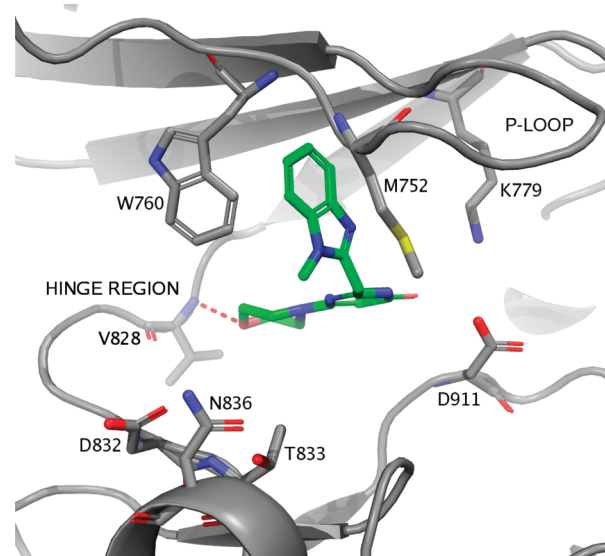


Figure 6. Binding of compound 8 to the ATP binding site of p110 δ (see Table 8 for X-ray data collection and refinement).

for LY294002, and several other previously reported^{20,25–27} morpholine containing compounds binding to PI3K γ or PI3K δ . In the P-loop, Met752 changed conformation relative to its position in the PI3K δ apo-structure, leaving space for the methyl-benzimidazole moiety to bind in the specificity pocket. The (R2) methyl group points toward residues at the entrance of the ATP binding site (Asp832, Thr833, and Asn836), however, leaving some space for larger substituents in PI3K δ . Interestingly, superposition between the X-ray structure of the PI3K δ -specific compound PIK-39 and the X-ray structure of compound 8 corroborated the observed SAR for the pyrimidone benzimidazole series. As exemplified by compounds 21, 22, and 23, there is a marked increase in PI3K δ potency over the other three isoforms when adding large substituents, comparable to the 2-methoxy phenyl in PIK-39, to the R2 position. The N–H of the amide in the pyrimidone

scaffold is pointing toward a partly solvent exposed region lined with Asp911 and Lys779, further supporting the hypothesis that small polar groups would be preferred over a methyl in this position. The original goal of this crystallography effort was to understand the structural basis for PI3K isoform specificity and to use the information to design more selective PI3K β inhibitors. However, from the structure of compound **8** bound to PI3K δ , one can observe that the large majority of residues in close contact with the inhibitor were conserved within the four isoforms. No specific interaction could explain on the one hand the pronounced affinity of the pyrimidone series for PI3K β and PI3K δ isoforms compared to PI3K α or PI3K γ and on the other hand the observed PI3K β specificity for compounds of these series. It has previously been suggested^{20,28} that differences in protein plasticity, particularly in the P-loop, would bring PI3K δ specificity for compounds occupying the specificity pocket. On the basis of the structural results for a PI3K β specific compound reported here, supported by the close sequence homology between PI3K β and PI3K δ relative to PI3K γ or PI3K α ,²⁹ we propose to extend this hypothesis by suggesting that not only PI3K δ but also PI3K β can readily adopt a conformation in which the specificity pocket is accessible for productive ligand binding. A conformation that would be energetically disfavored in the PI3K α and PI3K γ isoforms. To determine the veracity of this hypothesis and to clarify the origins of PI3K β versus PI3K δ specificity, further structural as well as thermodynamic studies of the class I PI3K isoforms and especially the p110 β , for which the first structure was recently solved,³⁰ would be of great value.

Cellular Selectivity. Activity of compound **8** on the four PI3K isoforms was further evaluated in cellular settings. To this end, the following cell-based assays, measuring Akt phosphorylation inhibition, were used to assess each isoform, PIK3CA-mutated H460 lung cancer cells for PI3K α , PTEN-deficient PC3 prostate cancer cells or MEF-3T3-myr p110 β mouse fibroblasts overexpressing activated p110 β for PI3K β , MEF-3T3-myr p110 δ mouse fibroblasts overexpressing p110 δ for PI3K δ and Raw264.7 mouse macrophages (after stimulation of Akt phosphorylation by C5a) for PI3K γ (Table 5).

Under these experimental conditions, compound **8** was shown to be at least 100-fold more potent on PI3K β than on PI3K α and PI3K γ isoforms and above 10-fold more potent over PI3K δ . In comparison, the reference compound TGX-221 exhibited roughly the same level of PI3K β selectivity versus

other isoforms. Compound **8** was shown to exhibit selectivity in cellular settings in agreement with what was observed in biochemical assays.

In Vivo Studies. Compound **8** was further evaluated in a pharmacokinetic (PK) study in female CB17/ICR-Prkdc severe combined immunodeficiency (SCID)/Crl mice showing an oral bioavailability of 26% (Table 6B). Pharmacokinetic parameters from the intravenous (iv) route (Table 6A) indicated a moderate clearance (3.1 L/h/kg) relative to hepatic blood flow (5.2 L/h/kg), a moderate Vdss (1.8 L/kg), and a long terminal elimination half-life ($T_{1/2}$ = 4.4 h).

Figure 7 illustrates that compound **8** has comparable exposure when administered at 6 mg/kg iv in solution and at 10 mg/kg po in suspension and similar terminal half-life.

Given the clear potential of compound **8** to selectively inhibit PI3K β in PTEN-deficient tumor cells and its favorable pharmacokinetic properties, its in vivo activity was evaluated in a mouse pharmacodynamic (PD) experiment. Compound **8** was administered orally at 300 mg/kg in SCID mice bearing human PTEN-deficient PC3 prostate carcinoma tumors, and a kinetic PK/PD test was performed harvesting tumor and plasma samples at 0.5, 1, 3, 6, and 24 h post dose. Target modulation in tumor tissue was assessed by measuring Akt phosphorylation on T308 residue. Figure 8A illustrates pAkt (T308) (bar graph, left axis) and the observed plasma concentrations of compound **8** (blue curve, right axis) at each time point. Tumor concentrations were also measured in this study and were found to be 1–3-fold lower than plasma concentrations (Table 7).

This experiment revealed a sustained and potent target inhibition induced by treatment with compound **8**, with more than 50% pAkt (T308) inhibition for at least 6 h (Figure 8a). This effect did correlate directly with compound exposure. A curve of plasma or tumor concentration versus percent inhibition of Akt phosphorylation is shown in Figure 8B and revealed a direct PK-PD response model. The in vivo effective concentration giving 50% PD modulation (EC_{50}) calculated from different experiments was estimated to be around 2 μ M (1.6 μ M for plasma concentrations and 2.1 μ M for tumor concentrations).

A kinetic PK/PD experiment was also performed after repeated administration of compound **8** for four days with two different dosing schedules, qd or bid. This experiment demonstrated the maintenance of pAkt (T308) inhibition over 24 h with the bid dosing at 300 mg/kg. Plasma concentrations at day 1 and day 4 were comparable at the different time points tested, indicating that there was neither compound accumulation due to inhibition of its own metabolism nor clearance related to autoinduction over four days (data not shown). This experiment supported the bid scheduling for the maintenance of continuous inhibition of Akt phosphorylation.

To determine the functional consequence of PI3K β inhibition, we then investigated the antitumor activity of compound **8** in human PTEN-deficient PC3 prostate carcinoma tumor model subcutaneously xenografted in SCID mice. In this study, tumors were allowed to reach at least 100 mm³ before compound or vehicle (control curve) administration, and tumor volume was measured regularly over the treatment period. Administered orally at 300 mg/kg bid for 9 days in PC3 tumor-bearing mice, compound **8** reduced tumor growth with a $\Delta T/\Delta C$ = 45% on day 32 at the end of the treatments (p = 0.0214) (Figure 9).

Table 5. Biochemical and Cellular PI3K β -Selectivity vs Other Isoforms: (A) Compound **8, (B) TGX-221**

		(A)			
compd 8	IC ₅₀ (nM) ^b	PI3K α	PI3K β	PI3K δ	PI3K γ
biochemistry	>10000	99 (LE = 0.40)		1395	>10000
cellular	>10000 ^a	76 ^a		2655 ^a	>10000 ^a
		86 ^a			
		(B)			
TGX-221	IC ₅₀ (nM) ^b	PI3K α	PI3K β	PI3K δ	PI3K γ
biochemistry	>10000		30	851	>10000
cellular	>1000 ^a		10 ^a	252 ^a	>1000 ^a
			11 ^a		

^apAkt-S473 was measured by MSD technology in H460, PC3, MEF-3T3-Myr p110 β , MEF-3T3-Myr p110 δ , and Raw264.7 cells, respectively. ^bIC₅₀ values are reported as the mean from at least two independent experiments, see Experimental Methods for assay details.

Table 6. Pharmacokinetic Parameters of Compound 8 in Female SCID Mice: (A) After a Single Intravenous Administration of 6 mg/kg in Solution in 10% Glycofurol, 5% PS80 in Glucose 5%, (B) After a Single Oral Administration of 10 mg/kg in Suspension in 0.6% Methylcellulose, 0.5% Tween 80

(A)							
compd 8 iv (6 mg/kg)							
C_0 (ng/mL)	$AUC_{(0-T_{last})}$ (h·ng/mL)	T_{last} (h)	$AUC_{(0-24 h)}$ (h·ng/mL)	$AUC_{(0-inf)}$ (h·ng/mL)	$T_{1/2}$ (h)	Cl (L/h/kg)	V_{dss} (L/h/kg)
4870	1950	24	1950	1950	4.4	3.1	3.1
(B)							
compd 8 po (10 mg/kg in suspension)							
C_{max} (ng/mL)	T_{max} (h)	$AUC_{(0-T_{last})}$ (h·ng/mL)	T_{last} (h)	$AUC_{(0-24 h)}$ (h·ng/mL)	$AUC_{(0-inf)}$ (h·ng/mL)	$T_{1/2}$ (h)	F (%)
641	0.5	846	24	846	850	3.9	26

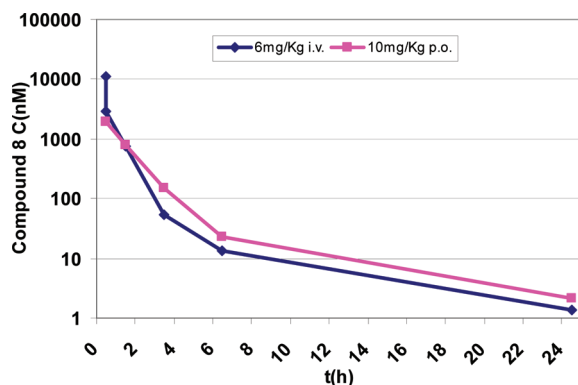


Figure 7. Time course exposure (logarithmic scale) of compound 8 after a single intravenous and oral administration to female SCID mice (arithmetic means for plasma, $n = 3$).

In this study, treatment with compound 8 induced tumor growth delay at well tolerated doses, with no sign of toxicity and no body weight loss. These results are in agreement with the published data in which downregulation of PIK3CB using a shRNA leads to PI3K pathway modulation and tumor growth inhibition selectively in PTEN-deficient genetic context (reported $T/C = 49\%$).⁵ Remarkably, compound 8 and

Table 7. PK Exposure from Compound 8 PK/PD Study in PC3 Mice Xenograft Model

	dose 300 mg/kg po				
time (h)	0.5	1	3	6	24
plasma (μM)	28	22	8	11	1.7
tumor (μM)	13	16	6	3.6	0.7

shRNA against PIK3CB led to a comparable tumor growth delay in PC3 model.

CHEMISTRY

As shown in Scheme 1, the 2-[4-(morpholin-4-yl)-6-oxo-1,6-dihydropyrimidin-2-yl]-*N*-phenylacetamide **5**¹³ can be obtained from the carboxylate **2** by condensation of aniline in the presence of 1-ethyl-3-(3-dimethylaminopropyl)carbodiimide (EDCI) and pyridine in dimethylformamide (DMF). The novel intermediate **1**¹³ was efficiently obtained by a one-pot reaction between morpholine and an excess (superior to 2 equiv) of commercially available ethyl 3-amino-3-ethoxyacrylate hydrochloride in the presence of *N,N*-diisopropylethylamine (DIPEA) in ethanol under reflux. Reactions reported in the literature use stoichiometric amount of morpholine and ethyl 3-amino-3-ethoxyacrylate hydrochloride and were intended to

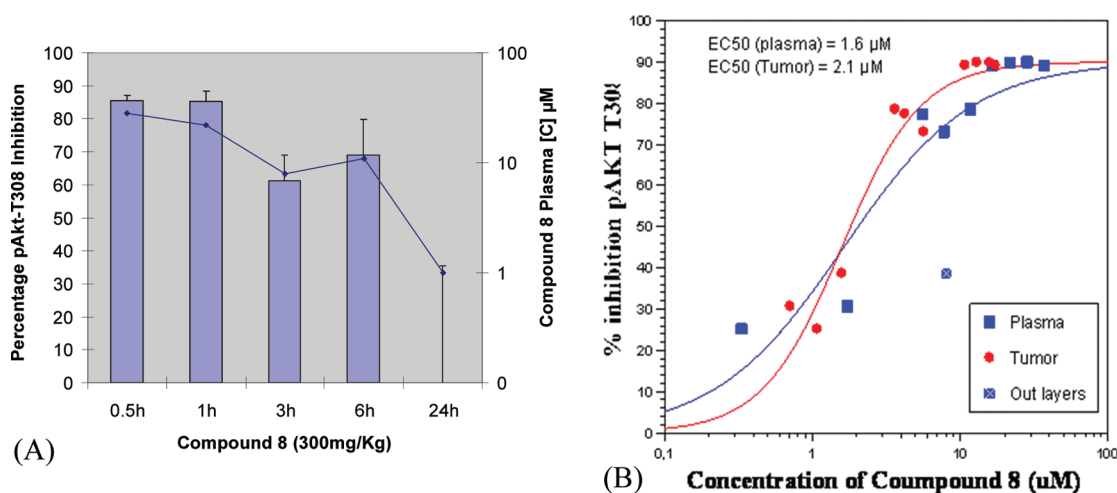


Figure 8. Effect of compound 8 on pAkt T308 inhibition. (A) In SCID mice PC3 xenograft model at 300 mg/kg po in suspension (percentage of pAkt-T308 inhibition on the left Y axis (bars reported represent the mean percentage and standard error of the mean of 3 mice per group) and plasma concentration [C] in μM log scale on the right Y axis). (B) EC_{50} measured by plotting concentration (plasma and tumor) vs inhibitory effect on pAkt-T308. $E = E_{max}C/EC_{50} + C$, where E denotes compound 8 effect on biomarker; E_{max} , the maximal effect of the compound on biomarker; C , compound 8 concentration in μM ; EC_{50} , the plasma or tumor concentration corresponding to the half-maximal response of the biomarker pAkt-T308.

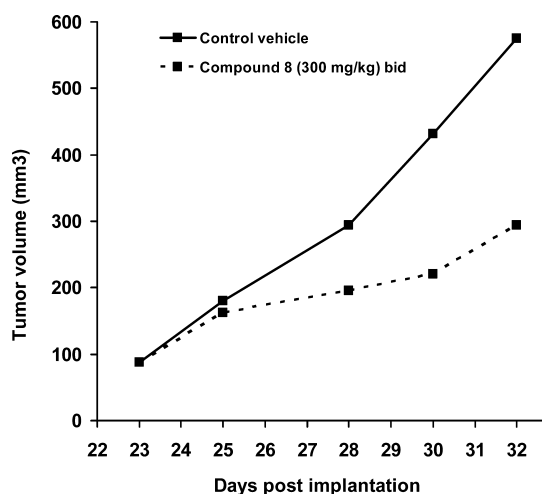


Figure 9. Compound 8 antitumor efficacy in mice PC3 xenograft model.

stop at the amidine intermediate (between brackets in Scheme 1) which can be isolated as the hydrochloride.^{31–35} In our case, the use of 3 equiv of imidate combined with the introduction of DIPEA led to the isolation of the novel ester **1**, formed most likely through condensation of the intermediate amidine with a second equivalent of imidate. Compound **1** was converted into **3** via methylation with methyl iodide in dioxane in the presence of cesium carbonate at 40 °C under argon. The two sodium salts **2** and **4** were obtained at room temperature by hydrolysis of the esters **1** and **3**, respectively, in tetrahydrofuran with 1 equiv of sodium hydroxide. The acids were isolated and conserved as the sodium salt because it was noticed that the acid has the tendency to decarboxylate even a room temperature.

The benzimidazoles **6**, **8–10**, **13–17**, **19–24**, and **27–28** were synthesized in two steps (Scheme 2). The condensation of the carboxylates **2** and **4** with the corresponding substituted diamines followed by an intramolecular cyclization in acetic

acid at reflux led to the expected benzimidazoles in variable yields (see Experimental Methods for details).

Alternatively, the benzimidazoles **11**, **12**, **18**, **25**, and **26** were isolated after alkylation of the benzimidazole moiety with alkyl halides in the presence of sodium hydroxide in acetone (Scheme 3).

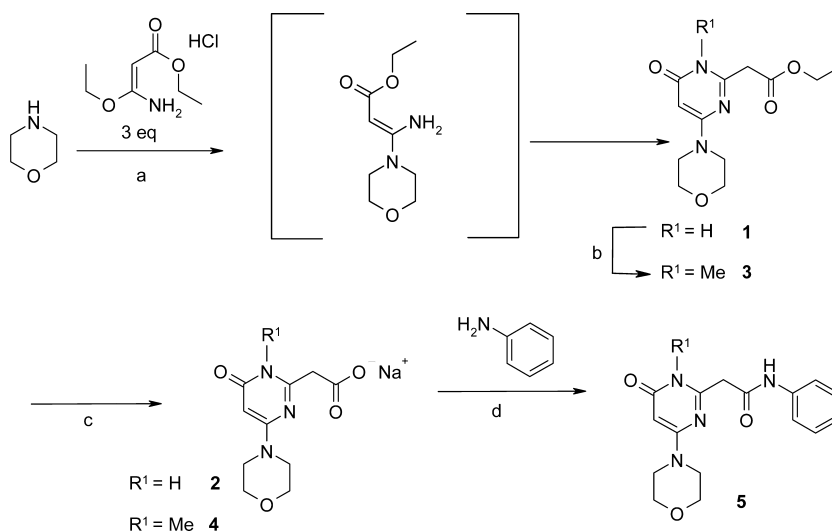
As shown in Scheme 4, the benzoxazoles **7**, **29–38**, **40**, **42**, and **45** were synthesized in two steps. The condensation of the carboxylates **2** and **4** with the corresponding substituted aminophenols followed by an intramolecular cyclization in *o*-xylene in the presence of *p*-toluenesulfonic acid (PTSA) at reflux led to the expected benzoxazole compounds in variable yields (see Experimental Methods for details).

Scheme 5 shows how the substituted benzoxazoles **39**, **41**, **43**, and **44** were synthesized from **38** by a Suzuki cross-coupling reaction with the corresponding boronic acids (or esters). The reactions were performed in 1,2-dimethoxyethane (DME) and water in the presence of sodium carbonate and tetrakis (triphenylphosphine) palladium(0) (Pd(PPh₃)₄) catalyst under argon atmosphere. The corresponding substituted benzoxazoles were obtained in moderate yield after column chromatography.

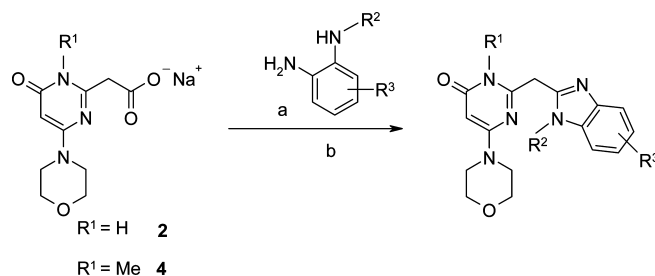
CONCLUSION

We have discovered a new series of high LE benzimidazole and benzoxazole pyrimidones as potent and selective PI3K β inhibitors which have been prepared by a new short and efficient synthesis, utilizing the novel intermediate compound **1**. Optimization of the series, through SAR analysis, physicochemical and in vitro pharmacokinetic optimization has led to the identification of compound **8**. Crystallized in PI3K δ , this molecule takes a conformation likely equivalent to the one it could adopt in PI3K β and that sheds light on important features in pyrimidone series SAR and on PI3K β isoform specificity. Compound **8** was found to be a potent and selective PI3K β inhibitor in biochemical and cellular settings. It demonstrated good selectivity versus other class I PI3K isoforms but also versus a large panel of protein kinases. This molecule was shown to potently inhibit Akt phosphorylation in

Scheme 1. Synthesis of Compound **5** and Intermediates **1–4**^a

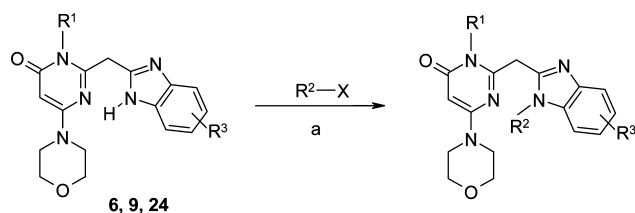


^aReagents and conditions: (a) DIPEA, EtOH, reflux, 24 h, 46%; (b) MeI, Cs₂CO₃, dioxane, 40 °C, 16 h, 75%; (c) NaOH, THF, rt, 48 h, 100%; (d) EDCl, pyridine, DMF, rt, 16 h, 70%.

Scheme 2. Synthesis of Benzimidazoles 6, 8–10, 13–17, 19–24, 27, and 28 from Table 1^a

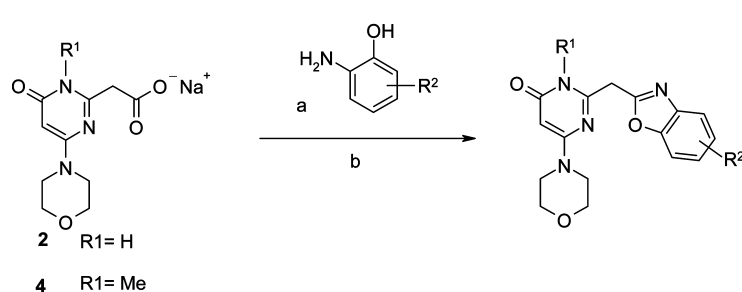
- 6:** $\text{R}^1 = \text{H}, \text{R}^2 = \text{H}, \text{R}^3 = \text{H}$
8: $\text{R}^1 = \text{H}, \text{R}^2 = \text{Me}, \text{R}^3 = \text{H}$
9: $\text{R}^1 = \text{H}, \text{R}^2 = \text{H}, \text{R}^3 = 5\text{-F}$
10: $\text{R}^1 = \text{Me}, \text{R}^2 = \text{H}, \text{R}^3 = 5\text{-F}$
13: $\text{R}^1 = \text{H}, \text{R}^2 = \text{H}, \text{R}^3 = 5\text{-Br}$
14: $\text{R}^1 = \text{H}, \text{R}^2 = \text{H}, \text{R}^3 = 5\text{-Cl}$
15: $\text{R}^1 = \text{H}, \text{R}^2 = \text{H}, \text{R}^3 = 5\text{-Me}$
16: $\text{R}^1 = \text{H}, \text{R}^2 = \text{H}, \text{R}^3 = 5\text{-OMe}$
17: $\text{R}^1 = \text{H}, \text{R}^2 = \text{H}, \text{R}^3 = 5\text{-CF}_3$
19: $\text{R}^1 = \text{H}, \text{R}^2 = \text{cyclopropyl}, \text{R}^3 = \text{H}$
20: $\text{R}^1 = \text{H}, \text{R}^2 = \text{-EtOMe}, \text{R}^3 = \text{H}$
21: $\text{R}^1 = \text{H}, \text{R}^2 = \text{cyclohexyl}, \text{R}^3 = \text{H}$
22: $\text{R}^1 = \text{H}, \text{R}^2 = \text{Ph}, \text{R}^3 = \text{H}$
23: $\text{R}^1 = \text{H}, \text{R}^2 = \text{-CH}_2\text{Ph}, \text{R}^3 = \text{H}$
24: $\text{R}^1 = \text{H}, \text{R}^2 = \text{H}, \text{R}^3 = 4\text{-Ph}$
27: $\text{R}^1 = \text{H}, \text{R}^2 = \text{Me}, \text{R}^3 = 5\text{-Ph}$
28: $\text{R}^1 = \text{H}, \text{R}^2 = \text{Me}, \text{R}^3 = 6\text{-Ph}$

^aReagents and conditions: (a) EDCI, pyridine, DMF, rt, 16 h; (b) AcOH, reflux, 4 h, overall yield 4–66%

Scheme 3. Preparation of Benzimidazoles 11, 12, 18, 25, and 26^a

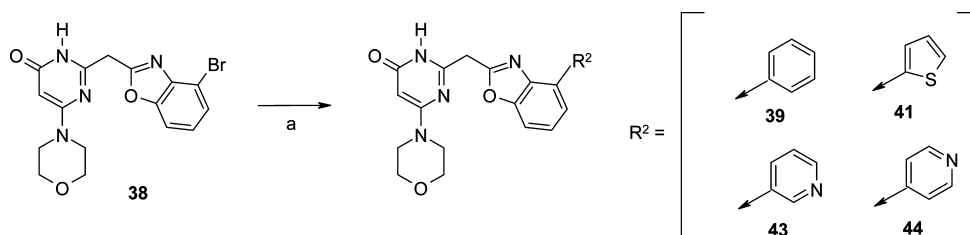
- 11:** $\text{R}^1 = \text{H}, \text{R}^2 = \text{Me}, \text{R}^3 = 5\text{-F}$
12: $\text{R}^1 = \text{H}, \text{R}^2 = \text{Me}, \text{R}^3 = 6\text{-F}$
18: $\text{R}^1 = \text{H}, \text{R}^2 = \text{Et}, \text{R}^3 = \text{H}$
25: $\text{R}^1 = \text{H}, \text{R}^2 = \text{Me}, \text{R}^3 = 4\text{-Ph}$
26: $\text{R}^1 = \text{H}, \text{R}^2 = \text{Me}, \text{R}^3 = 7\text{-Ph}$

^aReagents and conditions: (a) NaOH, Acetone, rt, 16 h.

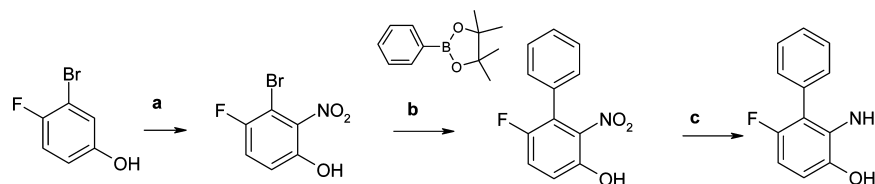
Scheme 4. Synthesis of Benzoxazoles 7, 29–38, 40, 42, and 45 from Table 2^a

- 7:** $\text{R}^1 = \text{H}, \text{R}^2 = \text{H}$
29: $\text{R}^1 = \text{H}, \text{R}^2 = 4\text{-F}$
30: $\text{R}^1 = \text{H}, \text{R}^2 = 5\text{-F}$
31: $\text{R}^1 = \text{H}, \text{R}^2 = 6\text{-F}$
32: $\text{R}^1 = \text{H}, \text{R}^2 = 7\text{-F}$
33: $\text{R}^1 = \text{Me}, \text{R}^2 = \text{H}$
34: $\text{R}^1 = \text{H}, \text{R}^2 = 4\text{-Me}$
35: $\text{R}^1 = \text{H}, \text{R}^2 = 5\text{-Me}$
36: $\text{R}^1 = \text{H}, \text{R}^2 = 6\text{-Me}$
37: $\text{R}^1 = \text{H}, \text{R}^2 = 7\text{-Me}$
38: $\text{R}^1 = \text{H}, \text{R}^2 = 4\text{-Br}$
40: $\text{R}^1 = \text{H}, \text{R}^2 = 7\text{-Ph}$
42: $\text{R}^1 = \text{H}, \text{R}^2 = 4\text{-pyridin-2-yl}$
45: $\text{R}^1 = \text{H}, \text{R}^2 = 4\text{-Ph}, 5\text{-F}$

^aReagents and conditions: (a) EDCI, pyridine, DMF, rt, 16 h; (b) PTSA, *o*-xylene, reflux, 5 h, overall yield 2–67%.

Scheme 5. Preparation of Benzoxazoles 39, 41, 43, and 44^a

^aReagents and conditions: (a) ArB(OH)_2 , $\text{Pd(PPh}_3)_4$, Na_2CO_3 , DME, H_2O , 100 °C, 5 h, yield 15–53%

Scheme 6. Preparation of 2-Amino-6-fluorobiphenyl-3-ol^a

^aReagents and conditions: (a) $(\text{NH}_4)_2\text{Ni}(\text{SO}_4)_2 \cdot 6\text{H}_2\text{O}$, HNO_3 , rt, 20 min. 31%; (b) $\text{Pd}(\text{dppf})\text{Cl}_2$, Cs_2CO_3 , dioxane/water, 95 °C, 5 h, 88%; (c) Fe, AcOH , 70 °C, 30 min. 78%.

PTEN-deficient PC3 prostate carcinoma cell line. In addition, it proved to exhibit good PK properties, allowing sustained PI3K pathway modulation and tumor growth delay in PTEN-deficient tumor xenografts. The biological profile of this molecule validated the benzimidazole and benzoxazole pyrimidone series as small molecules able to slow down the growth of PTEN-deficient tumors *in vivo* by targeting PI3K β kinase activity selectively. These results have a strong impact for the ongoing efforts to discover drugs targeting the PI3K pathway with new profiles. Isoform-selective compounds targeting only the relevant PI3K isoform for a given genetic context should avoid toxicities linked to unnecessary target inhibition and should provide a larger therapeutic index. It is certainly conceivable that the dependence of PTEN-deficient tumors on PI3K β is highly dependent on the presence of other genetic abnormalities and that this approach will have to be combined with other targeted therapies to reach tumor regressions in a more complex genetic context encountered in the majority of human cancer diseases.

EXPERIMENTAL METHODS

Chemistry. The nomenclature of the compounds was performed using ACDLABS software, Version 11.01.

All solvents and reagents obtained from commercial sources were used without further purification.

Thin layer chromatography was carried out on Merck silica gel 60 F254 glass plates. Flash chromatography was performed using prepacked Merck silica gel cartridges (15–40 μm).

The microwave apparatus used is a Biotage, Initiator 2.0, 400 W max, 2450 MHz instrument.

The ¹H NMR spectra at 400 MHz and the ¹³C NMR spectra at 500 MHz were performed on a Bruker Avance DRX-400 or Bruker Avance DPX-500 spectrometer with the chemical shifts (δ in ppm) in the solvent dimethyl sulfoxide-*d*₆ (DMSO-*d*₆) referenced at 2.5 ppm at a temperature of 303 K and coupling constants (*J*) were given in hertz.

The mass spectra (MS) were obtained by methods A–C:

Method A. Waters UPLC-SQD instrument; ionization, positive and/or negative mode electrospray (ES \pm). Chromatographic conditions: column, Acquity BEH C₁₈ 1.7 μm , 2.1 mm \times 50 mm. Solvents: A, H₂O (0.1% formic acid); B, CH₃CN (0.1% formic acid); column temperature, 50 °C; flow rate, 1 mL/min; gradient (2 min), from 5 to 50% of B in 0.8 min; 1.2 min, 100% of B; 1.85 min, 100% of B; 1.95, 5% of B; retention time = *T_r* (min).

Method B. Waters ZQ instrument; ionization, positive and/or negative mode electrospray (ES \pm). Chromatographic conditions: column, XBridge C₁₈ 2.5 μm , 3 mm \times 50 mm. Solvents: A, H₂O (0.1% formic acid); B, CH₃CN (0.1% formic acid); column temperature, 70 °C; flow rate, 0.9 mL/min; gradient (7 min), from 5% to 100% of B in 5.3 min; 5.5 min, 100% of B; 6.3 min, 5% of B; retention time = *T_r* (min).

Method C. Waters UPLC instrument, BEH C18 column, 2.1 mm \times 50 mm; 1.7 μm , H₂O + 0.1%TFA:AcN + 0.08% TFA 95:5 (0 min) to 5:95 (1.1 min) to 5:95 (1.7 min) to 95:5 (1.8 min) to 95:5 (2 min), 0.9 mL/min 55 °C; Waters SQD single quadrupole, 0.5 s scan time for mass 120–1200; retention time = *T_r* (min).

Table 8. X-Ray Data Collection and Refinement Statistics for Compound 8^a

Data Collection	
space group	P21
unit cell dimensions	
<i>a</i> , <i>b</i> , <i>c</i> (Å)	63.4, 220.5, 78.3
α , β , γ (deg)	90, 113.9, 90
resolution (Å)	71.57–2.80 (2.87–2.80)
total reflections	157600
unique reflections	47547
completeness (%)	98.4 (99.5)
<i>R</i> _{sym}	7.3 (47.1)
<i>I</i> / σ (<i>I</i>)	10.1 (2.4)
Refinement	
reflections used	47377
<i>R</i> / <i>R</i> _{free}	25.2/27.7
average <i>B</i> -values (Å ²)	74.8
no. of atoms	
protein	12514
ligand	82
solvent	34
rms deviations	
bond lengths (Å)	0.007
bond angles (deg)	0.87

^aData in parentheses correspond to the highest resolution shells. To calculate *R*_{free}, 5% of the reflections were excluded from the refinement. *R*_{sym} was defined as $R_{\text{sym}} = \frac{\sum_{hkl} \sum_i |I_i(hkl) - \langle I(hkl) \rangle|}{\sum_{hkl} \sum_i I_i(hkl)}$. rms, root mean square deviation.

Purities for final compounds were measured using ¹H NMR or LC (UV detection at 220 nm) and are >95% unless otherwise noted.

Ethyl [4-(Morpholin-4-yl)-6-oxo-1,6-dihydropyrimidin-2-yl]acetate (1). Ethyl 3-ethoxy-3-iminopropanoate hydrochloride (168.5 g (864 mmol)) and 155 mL (891 mmol) of *N,N*-diisopropylethylamine in 200 mL of ethanol were added to a solution of 25 g (287 mmol) of morpholine in 400 mL of ethanol heated to 95 °C. The reaction mixture was heated at 95 °C for 30 h and then allowed to return to ambient temperature. The precipitate formed was filtered off through sintered glass and then washed with 100 mL of ethanol, twice 500 mL of water, and finally, 500 mL of diethylether. The solid was dried under vacuum to give **1** (35 g, 46%) as a white solid. ¹H NMR (400 MHz): 1.19 (t, *J* = 7.1 Hz, 3 H), 3.38–3.44 (m, 4 H), 3.56 (s, 2H), 3.61 (dd, *J* = 4.0 and 5.7 Hz, 4 H), 4.12 (q, *J* = 7.1 Hz, 2 H), 5.20 (s, 1 H), 11.69 (br s, 1 H). Mass spectrometry: method A, *T_r* (min) = 0.48; $[M + H]^+$, *m/z* 268; $[M - H]^-$, *m/z* 266.

Sodium [4-(Morpholin-4-yl)-6-oxo-1,6-dihydropyrimidin-2-yl]acetate (2). Sodium hydroxide (18.7 mL (1 equiv), 2 M) were added to a solution of 10 g (37 mmol) of **1** in 300 mL of tetrahydrofuran. The reaction mixture was stirred for 48 h at ambient temperature. The precipitate formed was filtered off through sintered glass, washed with ethyl acetate, and rinsed several times with diethyl ether. The solid obtained was then dried under vacuum to give **2** (8.7 g, 89%) as a white solid. ¹H NMR (400 MHz): 3.08 (s, 2 H), 3.38 (t, *J* = 4.6 Hz, 4 H), 3.61 (t, *J* = 4.6 Hz, 4 H), 5.08 (s, 1 H), 13.16 (br s, 1

H). MS: method A, T_r (min) = 0.29; $[M + H]^+$, m/z 240; $[M - H]^-$, m/z 238.

Ethyl [1-Methyl-4-(morpholin-4-yl)-6-oxo-1,6-dihydropyrimidin-2-yl]acetate (3). To a suspension of 500 mg (1.9 mmol) of **1** in 15 mL of dioxane were added 330 mg (2.4 mmol) of potassium carbonate and 0.15 mL (2.3 mmol) of methyl iodide. The reaction mixture was heated at 40 °C for 16 h and then cooled to ambient temperature. The suspension was filtered through sintered glass and then rinsed with dioxane, and the filtrate was concentrated under reduced pressure. The residue was purified by silica column chromatography, elution being carried out with a mixture of dichloromethane, acetonitrile, and methanol (98/01/01, 96/02/02, then 90/05/05 V/V/V) to give **3** (200 mg, 38%) as a white solid. $^1\text{H NMR}$ (400 MHz): 1.21 (t, $J = 7.2$ Hz, 3 H), 3.28 (s, 3H), 3.40 (m, 4 H), 3.61 (m, 4 H), 3.92 (s, 2H), 3.61 (q, $J = 7.2$ Hz, 2H), 5.35 (s, 1 H). MS: method A, T_r (min) = 0.53; $[M + H]^+$, m/z 282; $[M - H]^-$, m/z 280.

Sodium [1-Methyl-4-(morpholin-4-yl)-6-oxo-1,6-dihydropyrimidin-2-yl]acetate (4). Sodium hydroxide (13.74 mL (1 equiv), 2 M) were added to a solution of 7.73 g (27.5 mmol) of **2** in 200 mL of tetrahydrofuran. The reaction mixture was stirred for 48 h at ambient temperature. The precipitate formed was filtered through sintered glass, washed with ethyl acetate, and rinsed several times with diethyl ether. The solid obtained was then dried under vacuum to give **4** (7.56 g; 100%) as a white solid. $^1\text{H NMR}$ (400 MHz): 3.29–3.33 (m, partially masked, 5 H), 3.38 (t, $J = 4.7$ Hz, 4 H), 3.61 (t, $J = 4.7$ Hz, 4 H), 5.24 (s, 1 H). MS: method B, T_r (min) = 1.67; $[M + H]^+$, m/z 254; $[M - H]^-$, m/z 252.

2-[4-(Morpholin-4-yl)-6-oxo-1,6-dihydropyrimidin-2-yl]-*N*-phenylacetamide (5). **2** (1.04 g (4 mmol)) were introduced into 16 mL of dimethylformamide, and then 0.65 mL (8 mmol) of pyridine, 1.0 g (5.2 mmol) of *N*-[3-(dimethylamino)propyl]-*N'*-ethylcarbodiimide hydrochloride (EDCI), and 0.75 g (8.1 mmol) of aniline were added. The reaction mixture was stirred at ambient temperature overnight and then evaporated to dryness under reduced pressure. Water and ethyl acetate were added, and the resulting mixture was thus stirred for 30 min. The precipitate formed was filtered off, washed with diethyl ether, and dried to give **5** (879 mg, 70%) as a beige solid. $^1\text{H NMR}$ (400 MHz): 3.38–3.44 (m, 4 H), 3.56–3.63 (m, 6 H), 5.20 (s, 1H), 7.06 (t, $J = 7.8$ Hz, 1 H), 7.31 (t, $J = 8.6$ Hz, 2 H), 7.56 (d, $J = 8.6$ Hz, 2 H), 10.14 (s, 1 H), 11.64 (br s, 1H). MS: method A, T_r (min) = 0.55; $[M + H]^+$, m/z 315; $[M - H]^-$, m/z 313.

2-(1*H*-Benzimidazol-2-ylmethyl)-6-(morpholin-4-yl)pyrimidin-4(3*H*)-one (6). To a suspension of 300 mg (1.1 mmol) of **2** in a mixture of 2.5 mL of dimethylformamide and 2.5 mL of pyridine, 330 mg (1.7 mmol) of *N*-[3-(dimethylamino)propyl]-*N'*-ethylcarbodiimide hydrochloride and 248 mg (2.3 mmol) of benzene-1,2-diamine were added. The reaction mixture was stirred at ambient temperature overnight and then evaporated to dryness under reduced pressure. The residue was taken up in 5 mL of acetic acid and brought to reflux for 1 h and then concentrated under reduced pressure. Then 100 mL of water were added and a saturated aqueous solution of sodium bicarbonate was added until a pH around 7 was obtained. The precipitate formed was filtered then purified by flash chromatography (dichloromethane/methanol: 90/10) to give **6** (75 mg, 21%) as a beige solid. $^1\text{H NMR}$ (400 MHz): 3.39 (m, 4 H), 3.58 (m, 4 H), 4.09 (s, 2 H), 5.21 (s, 1 H), 7.14 (m, 2 H), 7.50 (m, 2 H), 11.86 (br m, 2H). MS: method A; T_r (min) = 0.35; $[M + H]^+$, m/z 312; $[M - H]^-$, m/z 310.

2-(1,3-Benzoxazol-2-ylmethyl)-6-(morpholin-4-yl)pyrimidin-4(3*H*)-one (7). Pyridine (4 mL (49.7 mmol)), 550 mg (2.3 mmol) of EDCI, and 700 mg (6.4 mmol) of 2-aminophenol were added to a solution of 500 mg (1.9 mmol) of **2** in 4 mL of dimethylformamide. The reaction mixture was stirred at ambient temperature overnight and then evaporated to dryness under reduced pressure. Water and ethyl acetate were added, and the resulting mixture was thus stirred for 30 min. The precipitate formed was filtered off and rinsed with water, diethyl ether, and petroleum ether. The solid was dried under vacuum and then suspended in 60 mL of xylene, and 40 mg of 4-methylbenzenesulphonic acid hydrate were added. The reaction

mixture was brought to reflux overnight. After cooling to room temperature, the insoluble material formed was filtered off. The filtrate was concentrated to dryness under reduced pressure, and the residue was then purified by flash chromatography, eluent dichloromethane/methanol, 98/02 then 90/10 to give **7** (30 mg, 8%) as a white solid; mp 224 °C. $^1\text{H NMR}$ (400 MHz): 3.35 (t, $J = 5.0$ Hz, 4 H), 3.56 (t, $J = 4.9$ Hz, 4 H), 4.25 (s, 2 H), 5.25 (br s, 1 H), 7.31–7.40 (m, 2 H), 7.62–7.74 (m, 2 H), 11.92 (br s, 1 H). MS: method A, T_r (min) = 0.60; $[M + H]^+$, m/z 313; $[M - H]^-$, m/z 311.

2-[(1-Methyl-1*H*-benzimidazol-2-yl)methyl]-6-(morpholin-4-yl)pyrimidin-4(3*H*)-one (8). By a similar procedure to that described for the synthesis of **6** using 3 g (11.5 mmol) of **2** and 2.81 g (23 mmol) of *N*-methyl-1,2-phenylenediamine, **8** (2.05 g, 55%) was obtained as a white solid; mp 257 °C. $^1\text{H NMR}$ (400 MHz): 3.34 (m, 4 H), 3.56 (m, 4 H), 3.80 (s, 3 H), 4.20 (s, 2 H), 5.21 (s, 1 H), 7.17 (t, $J = 7.8$ Hz, 1 H), 7.23 (t, $J = 7.8$ Hz, 1 H), 7.52 (d, $J = 7.8$ Hz, 1 H), 7.56 (d, $J = 7.8$ Hz, 1 H), 11.85 (br s, 1 H). MS: method A, T_r (min) = 0.36; $[M + H]^+$, m/z 326; $[M - H]^-$, m/z 324.

2-[(5-Fluoro-1*H*-benzimidazol-2-yl)methyl]-6-(morpholin-4-yl)pyrimidin-4(3*H*)-one (9). By a similar procedure to that described for the synthesis of **6** using 7.00 g (26.8 mmol) of **2** and 6.76 g (53.6 mmol) of 1,2-diamino-4-fluorobenzene, **9** (3.00 g, 34%) was obtained as an off-white solid. $^1\text{H NMR}$ (400 MHz): 3.37 (t, $J = 4.9$ Hz, 4 H), 3.58 (t, $J = 4.9$ Hz, 4 H), 4.08 (s, 2 H), 5.22 (s, 1 H), 7.00 (t, $J = 8.2$ Hz, 1 H), 7.31 (dd, $J = 0.7$ and 9.8 Hz, 1 H), 7.49 (br s, 1 H), 12.15 (br s, 2 H). MS: method A, T_r (min) = 0.41; $[M + H]^+$, m/z 330; $[M - H]^-$, m/z 328.

2-[(5-Fluoro-1*H*-benzimidazol-2-yl)methyl]-3-methyl-6-(morpholin-4-yl)pyrimidin-4(3*H*)-one (10). By a similar procedure to that described for the synthesis of **6** using 400 mg (1.5 mmol) of **4** and 367 mg (2.9 mmol) of 1,2-diamino-4-fluorobenzene, **10** (75 mg, 15%) was obtained as an off-white solid, mp 265 °C. $^1\text{H NMR}$ (400 MHz): 3.36 (m, 4 H), 3.37 (s, 3 H), 3.57 (m, 4 H), 4.37 (s, 2 H), 5.37 (s, 1 H), 7.00 (dt, $J = 2.0$ and 9.0 Hz, 1 H), 7.31 (dd, $J = 2.0$ and 10.5 Hz, 1 H), 7.50 (dd, $J = 4.4$ and 9.0 Hz, 1 H), 12.43 (br m, 1 H).

2-[(5-Fluoro-1-methyl-1*H*-benzimidazol-2-yl)methyl]-6-(morpholin-4-yl)pyrimidin-4(3*H*)-one (11) and 2-[(6-Fluoro-1-methyl-1*H*-benzimidazol-2-yl)methyl]-6-(morpholin-4-yl)pyrimidin-4(3*H*)-one (12). Sodium hydroxide (2N) (0.75 mL (1.5 mmol)) was added to a solution of 329 mg (1 mmol) of **9** in 15 mL of acetone. After stirring at room temperature for 10 min, 93 μL (1.5 mmol) of iodomethane were added and the reaction mixture was stirred overnight. The solvent was evaporated to dryness under reduced pressure, the residue was diluted in 20 mL of water, and the medium was brought to pH 6 using hydrochloric acid (2N). After the insoluble material has been filtered off, the filtrate was evaporated to dryness under reduced pressure and purified by flash chromatography; eluent, dichloromethane/methanol 95/05 to give a 50/50 mixture of two isomers (145 mg, 42%). The two isomers were separated by chiral chromatography on Chiralpak AD 20 μm (1000 g, diameter 80 mm; mobile phase, ethanol/heptane/triethylamine 60/40/0.1; mobile phase flow rate, 150 mL/min; UV detection, 240 nm) to give **11** (55 mg, 16%) as an off-white solid. $^1\text{H NMR}$ (400 MHz): 3.31–3.36 (m, 4 H), 3.53–3.58 (m, 4 H), 3.80 (s, 3 H), 4.19 (s, 2 H), 5.21 (s, 1 H), 7.09 (ddd, $J = 2.5$ and 8.8 and 9.8 Hz, 1 H), 7.37 (dd, $J = 2.5$ and 9.8 Hz, 1 H), 7.54 (dd, $J = 4.8$ and 8.8 Hz, 1 H), 11.87 (br m, 1 H). MS: method A, T_r (min) = 0.44; $[M + H]^+$, m/z 344; $[M - H]^-$, m/z 342 and **12** (68 mg, 20%) as an off-white solid. $^1\text{H NMR}$ (400 MHz): 3.27–3.40 (m, partially masked, 4 H), 3.56 (m, 4 H), 3.78 (s, 3 H), 4.18 (s, 2 H), 5.21 (s, 1 H), 7.01 (m, 1 H), 7.44 (dd, $J = 2.5$ and 9.1 Hz, 1 H), 7.56 (dd, $J = 4.9$ and 8.8 Hz, 1 H), 11.74 (br m, 1 H). MS: method A, T_r (min) = 0.46; $[M + H]^+$, m/z 344; $[M - H]^-$, m/z 342.

2-[(5-Bromo-1*H*-benzimidazol-2-yl)methyl]-6-(morpholin-4-yl)pyrimidin-4(3*H*)-one (13). By a similar procedure to that described for the synthesis of **6** using 1.3 g (5 mmol) of **2** and 1.87 g (10 mmol) of 4-bromobenzene-1,2-diamine, **13** (0.56 g, 29%) was obtained as an off-white solid. $^1\text{H NMR}$ (400 MHz): 3.34–3.39 (m, 4 H), 3.55–3.59 (m, 4 H), 4.09 (s, 2 H), 5.21 (s, 1 H), 7.28 (dd, $J = 2.0$ and 8.6 Hz, 1 H), 7.47 (d, $J = 8.6$ Hz, 1 H), 7.71 (d, $J = 2.0$ Hz, 1 H),

12.20 (br m, 2 H). MS: method B, T_r (min) = 2.71; $[M + H]^+$, m/z 390; $[M - H]^-$, m/z 388.

2-[(5-Chloro-1H-benzimidazol-2-yl)methyl]-6-(morpholin-4-yl)pyrimidin-4(3H)-one (14). By a similar procedure to that described for the synthesis of **6** using 400 mg of **2** (1.5 mmol) and 436 mg (3.1 mmol) of 4-chlorobenzene-1,2-diamine, **14** (260 mg, 49%) was obtained as a white powder. 1H NMR (400 MHz): 3.37 (m, 4 H), 3.57 (m, 4 H), 4.10 (s, 2 H), 5.22 (s, 1 H), 7.17 (dd, $J = 1.9$ and 8.6 Hz, 1 H), 7.51 (d, $J = 8.6$ Hz, 1 H), 7.57 (d, $J = 1.9$ Hz, 1 H), 12.18 (br m, 2 H). MS: method A, T_r (min) = 0.51; $[M + H]^+$, m/z 346; $[M - H]^-$, m/z 344.

2-[(5-Methyl-1H-benzimidazol-2-yl)methyl]-6-(morpholin-4-yl)pyrimidin-4(3H)-one (15). By a similar procedure to that described for the synthesis of **6** using 65 mg (0.2 mmol) of **2** and 30 mg (0.2 mmol) of 3,4-diamino toluene, **15** (7 mg, 8%) was obtained as an off-white powder. 1H NMR (400 MHz): 2.44 (s, 3 H), 3.20–3.56 (m, 8 H), 4.45 (s, 2 H), 5.30 (s, 1 H), 7.25–7.70 (m, 3 H). MS: method C, T_r (min) = 0.74; $[M + H]^+$, m/z 326; $[M - H]^-$, m/z 324.

2-[(5-Methoxy-1H-benzimidazol-2-yl)methyl]-6-(morpholin-4-yl)pyrimidin-4(3H)-one (16). By a similar procedure to that described for the synthesis of **6** using 261 mg (1 mmol) of **2** and 166 mg (1.2 mmol) of 3,4-diaminoanisole, **16** (8 mg, 2%) was obtained as an off-white powder (purity = 90%). 1H NMR (400 MHz): 3.38 (m, 4 H), 3.58 (m, 4 H), 3.76 (s, 3 H), 4.04 (s, 2 H), 5.21 (s, 1 H), 6.72–6.82 (m, 1 H), 6.89–7.15 (br m, 1 H), 7.27–7.52 (br m, 1 H), 11.82 (br m, 1 H), 12.11 (br m, 1 H). MS: method A, T_r (min) = 0.40; $[M + H]^+$, m/z 342.

6-(Morpholin-4-yl)-2-[[5-(trifluoromethyl)-1H-benzimidazol-2-yl]methyl]pyrimidin-4(3H)-one (17). By a similar procedure to that described for the synthesis of **6** using 65 mg (0.2 mmol) of **2** and 44 mg (0.2 mmol) of 4-(trifluoromethyl)-1,2-phenylenediamine, **17** (15 mg, 16%) was obtained as an off-white powder. 1H NMR (400 MHz): 3.30 (m, 4 H), 3.53 (m, 4 H), 4.20 (s, 2 H), 5.25 (s, 1 H), 7.50 (m, 1 H), 7.75 (m, 1 H), 7.92 (s, 1 H). MS: method C, T_r (min) = 0.93; $[M + H]^+$, m/z 380; $[M - H]^-$, m/z 378.

2-[(1-Ethyl-1H-benzimidazol-2-yl)methyl]-6-(morpholin-4-yl)pyrimidin-4(3H)-one (18). By a similar procedure to that described for the synthesis of **11** or **12** using 155 mg (0.5 mmol) of **6**, 0.38 mL (0.76 mmol) of sodium hydroxide (2N) and 60 μ L (1 mmol) of iodoethane, **18** (30 mg, 18%) was obtained as a beige powder. 1H NMR (400 MHz): 1.31 (t, $J = 7.1$ Hz, 3 H), 3.34 (m, 4 H), 3.57 (m, 4 H), 4.18 (s, 2 H), 4.31 (q, $J = 7.1$ Hz, 2 H), 5.21 (s, 1 H), 7.13–7.19 (m, 1 H), 7.20–7.25 (m, 1 H), 7.51–7.59 (m, 2 H), 11.88 (br m, 1 H). MS: method A, T_r (min) = 0.42; $[M + H]^+$, m/z 340; $[M - H]^-$, m/z 338.

2-[(1-Cyclopropyl-5-fluoro-1H-benzimidazol-2-yl)methyl]-6-(morpholin-4-yl)pyrimidin-4(3H)-one (19). By a similar procedure to that described for the synthesis of **6** using 300 mg (1.1 mmol) of **2** and 645 mg (3.9 mmol) of N^1 -cyclopropyl-4-fluorobenzene-1,2-diamine, **19** (15 mg, 4%) was obtained as a white powder. 1H NMR (400 MHz): 1.04–1.22 (m, 4 H), 3.33–3.43 (m, 5 H), 3.54–3.60 (m, 4 H), 4.24 (s, 2 H), 5.22 (s, 1 H), 7.09 (dt, $J = 2.4$ and 9.3 Hz, 1 H), 7.39 (dd, $J = 2.4$ and 9.8 Hz, 1 H), 7.56 (dd, $J = 4.8$ and 9.3 Hz, 1 H), 11.80 (br m, 1 H). MS: method A, T_r (min) = 0.57; $[M + H]^+$, m/z 370; $[M - H]^-$, m/z 368.

2-[[5-Fluoro-1-(2-methoxyethyl)-1H-benzimidazol-2-yl]methyl]-6-(morpholin-4-yl)pyrimidin-4(3H)-one (20). By a similar procedure to that described for the synthesis of **6** using 300 mg (1.1 mmol) of **2** and 761 mg (4.1 mmol) of 4-fluoro- N^1 -(2-methoxyethyl)benzene-1,2-diamine hydrochloride, **20** (120 mg, 27%) was obtained as a white powder. 1H NMR (400 MHz): 3.20 (s, 3 H), 3.33–3.40 (m, 4 H), 3.54–3.59 (m, 4 H), 3.63 (t, $J = 5.3$ Hz, 2 H), 4.19 (s, 2 H), 4.47 (t, $J = 5.3$ Hz, 2 H), 5.21 (s, 1 H), 7.08 (dt, $J = 2.4$ and 9.3 Hz, 1 H), 7.37 (dd, $J = 2.4$ and 9.8 Hz, 1 H), 7.57 (dd, $J = 4.8$ and 9.3 Hz, 1 H), 11.80 (br m, 1 H). MS: method A, T_r (min) = 0.51; $[M + H]^+$, m/z 388; $[M - H]^-$, m/z 386.

2-[(1-Cyclohexyl-1H-benzimidazol-2-yl)methyl]-6-(morpholin-4-yl)pyrimidin-4(3H)-one (21). By a similar procedure to that described for the synthesis of **6** using 65 mg (0.2 mmol) of **2** and 47 mg (0.2 mmol) of N^1 -cyclohexyl-1,2-benzenediamine, **21** (27 mg,

27%) was obtained as an off-white powder. 1H NMR (400 MHz): 1.35–1.50 (m, 3 H), 1.67 (m, 1 H), 1.79–1.91 (m, 2 H), 2.15–2.30 (m, 2 H), 3.35 (m, 4 H), 3.48 (m, 4 H), 4.45–4.55 (m, 3 H), 5.28 (s, 1 H), 7.42 (m, 2 H), 7.78 (m, 1 H), 8.03 (m, 1 H). MS: method C, T_r (min) = 0.92; $[M + H]^+$, m/z 394; $[M - H]^-$, m/z 392.

6-(Morpholin-4-yl)-2-[(1-phenyl-1H-benzimidazol-2-yl)methyl]pyrimidin-4(3H)-one (22). By a similar procedure to that described for the synthesis of **6** using 300 mg (1.1 mmol) of **2** and 423 mg (2.3 mmol) of N -phenylbenzene-1,2-diamine, **22** (230 mg, 52%) was obtained as a white powder. 1H NMR (400 MHz): 3.32 (br m, 4 H), 3.56 (m, 4 H), 4.05 (s, 2 H), 5.16 (s, 1 H), 7.11–7.17 (m, 1 H), 7.19–7.30 (m, 2 H), 7.49–7.72 (m, 6 H), 11.74 (br m, 1 H). MS: method A, T_r (min) = 0.66; $[M + H]^+$, m/z 388; $[M - H]^-$, m/z 386.

2-[(1-Benzyl-1H-benzimidazol-2-yl)methyl]-6-(morpholin-4-yl)pyrimidin-4(3H)-one (23). By a similar procedure to that described for the synthesis of **6** using 300 mg of **2** and 455 mg (2.3 mmol) of N -benzylbenzene-1,2-diamine, **23** (250 mg, 54%) was obtained as a beige powder. 1H NMR (400 MHz): 3.25–3.35 (m partially masked, 4 H), 3.52–3.58 (m, 4 H), 4.18 (s, 2 H), 5.18 (s, 1 H), 5.56 (s, 2 H), 7.13–7.20 (m, 4 H), 7.23–7.35 (m, 3 H), 7.39–7.47 (m, 1 H), 7.55–7.64 (m, 1 H), 11.88 (br m, 1), MS: method A, T_r (min) = 0.58; $[M + H]^+$, m/z 402; $[M - H]^-$, m/z 400.

6-(Morpholin-4-yl)-2-[(4-phenyl-1H-benzimidazol-2-yl)methyl]pyrimidin-4(3H)-one (24). By a similar procedure to that described for the synthesis of **6** using 840 mg (3.2 mmol) of **2** and 730 mg (2.9 mmol) of 1,1'-biphenyl-2,3-diamine, **24** (455 mg, 40%) was obtained as a gray powder. 1H NMR (400 MHz): 3.22–3.42 (m partially masked, 4 H), 3.56 (m, 4 H), 4.14 (s, 2 H), 5.20 (s, 1 H), 6.93–8.26 (m, 8 H), 11.80 (br m, 1 H), 12.30 (br m, 1 H). MS: method A, T_r (min) = 0.61; $[M + H]^+$, m/z 388; $[M - H]^-$, m/z 386.

2-[(1-Methyl-4-phenyl-1H-benzimidazol-2-yl)methyl]-6-(morpholin-4-yl)pyrimidin-4(3H)-one (25) and 2-[(1-Methyl-7-phenyl-1H-benzimidazol-2-yl)methyl]-6-(morpholin-4-yl)pyrimidin-4(3H)-one (26). By a similar procedure to that described for the synthesis of **11** and **12** using 300 mg (0.8 mmol) of **24**, two compounds were obtained. **25** (57 mg, 20%) as an off-white solid. 1H NMR (400 MHz): 3.30 (m partially masked, 4 H), 3.54 (m, 4 H), 3.86 (s, 3 H), 4.28 (s, 2 H), 5.19 (s, 1 H), 7.25–7.62 (m, 6H), 8.04 (d, $J = 7.8$ Hz, 2 H), 11.93 (br m, 1 H). MS: method A, T_r (min) = 0.62; $[M + H]^+$, m/z 402; $[M - H]^-$, m/z 400. **26** (52 mg, 18%) as a white solid. 1H NMR (400 MHz): 3.32 (m, 7 H), 3.57 (m, 4 H), 4.31 (s, 2 H), 5.24 (s, 1 H), 7.16 (d, $J = 7.8$ Hz, 1 H), 7.36 (t, $J = 7.8$ Hz, 1 H), 7.42 (m, 2 H), 7.46–7.56 (m, 3 H), 7.70 (d, $J = 7.8$ Hz, 1 H), 11.96 (br m, 1 H). MS: method A, T_r (min) = 0.68; $[M + H]^+$, m/z 402; $[M - H]^-$, m/z 400.

2-[(1-Methyl-5-phenyl-1H-benzimidazol-2-yl)methyl]-6-(morpholin-4-yl)pyrimidin-4(3H)-one (27). By a similar procedure to that described for the synthesis of **6** using 733 mg (2.8 mmol) of **2** and 455 mg (2.3 mmol) of N -4-methyl-biphenyl-3,4-diamine, **27** (674 mg, 66%) was obtained as a white powder. 1H NMR (400 MHz): 3.35 (m, 4 H), 3.57 (m, 4 H), 3.83 (s, 3 H), 4.22 (s, 2 H), 5.22 (s, 1 H), 7.32 (t, $J = 7.8$ Hz, 1 H), 7.45 (t, $J = 7.8$ Hz, 2 H), 7.55 (d, $J = 8.5$ Hz, 1 H), 7.61 (d, $J = 8.5$ Hz, 1 H), 7.69 (d, $J = 7.8$ Hz, 2 H), 7.84 (s, 1 H), 11.89 (br m, 1 H). MS: method A, T_r (min) = 0.63; $[M + H]^+$, m/z 402; $[M - H]^-$, m/z 400.

2-[(1-Methyl-6-phenyl-1H-benzimidazol-2-yl)methyl]-6-(morpholin-4-yl)pyrimidin-4(3H)-one (28). By a similar procedure to that described for the synthesis of **6** using 710 mg (2.7 mmol) of **2** and 490 mg of N -3-methyl-biphenyl-2,3-diamine, **28** (440 mg, 44%) was obtained as an off-white powder. 1H NMR (400 MHz): 3.30–3.40 (m partially masked, 4 H), 3.55 (m, 4 H), 3.92 (s, 3 H), 4.34 (s, 2 H), 5.25 (s, 1 H), 7.37 (t, $J = 7.8$ Hz, 1 H), 7.49 (t, $J = 7.8$ Hz, 2 H), 7.61 (d, $J = 8.3$ Hz, 1 H), 7.70 (br d, $J = 8.3$ Hz, 1 H), 7.77 (d, $J = 7.8$ Hz, 2 H), 7.95 (s large, 1 H); 11.95 (br m, 1 H). MS: method A, T_r (min) = 0.67; $[M + H]^+$, m/z 402; $[M - H]^-$, m/z 400.

2-[[4-Fluoro-1,3-benzoxazol-2-yl)methyl]-6-(morpholin-4-yl)pyrimidin-4(3H)-one (29). By a similar procedure to that described for the synthesis of **7** using 500 mg (1.9 mmol) of **2** and 357 mg (2.8 mmol) of 2-amino-3-fluorophenol, **32** (110 mg, 17%) was obtained as a white solid. 1H NMR (400 MHz): 3.35 (m, 4 H), 3.56 (m, 4 H), 4.29 (s, 2 H), 5.26 (s, 1 H), 7.25 (dd, $J = 8.3$ and 10.2 Hz, 1

H), 7.42 (dt, $J = 5.1$ and 8.3 Hz, 1 H), 7.60 (d, $J = 8.3$ Hz, 1 H), 11.93 (br s, 1 H). MS: method A, T_r (min) = 0.64; $[M + H]^+$, m/z 331; $[M - H]^-$, m/z 329.

2-[(5-Fluoro-1,3-benzoxazol-2-yl)methyl]-6-(morpholin-4-yl)pyrimidin-4(3H)-one (30). By a similar procedure to that described for the synthesis of 7 using 1 g (3.8 mmol) of 2 and 466 mg (3.7 mmol) of 2-amino-4-fluorophenol, 30 (188 mg, 15%) was obtained as a brown solid. $^1\text{H NMR}$ (400 MHz): for this product, all the signals were broad, with: 3.33–3.39 (m, 4 H), 3.54–3.62 (m, 4 H), 4.26 (s, 2 H), 5.25 (s, 1 H), 7.25 (t, $J = 9.0$ Hz, 1 H), 7.61 (d, $J = 9.0$ Hz, 1 H), 7.76 (dd, $J = 4.5$ and 9.0 Hz, 1 H), 11.83–11.96 (br m, 1 H). MS: method A, T_r (min) = 0.65; $[M + H]^+$, m/z 331; $[M - H]^-$, m/z 329.

2-[(6-Fluoro-1,3-benzoxazol-2-yl)methyl]-6-(morpholin-4-yl)pyrimidin-4(3H)-one (31). By a similar procedure to that described for the synthesis of 7 using 550 mg (2.1 mmol) of 2 and 815 mg (6.4 mmol) of 2-amino-5-fluorophenol, 31 (15 mg, 2%) was obtained as a white solid; $^1\text{H NMR}$ (400 MHz): 3.35 (m, 4 H), 3.56 (m, 4 H), 4.25 (s, 2 H), 5.25 (br s, 1 H), 7.24 (ddd, $J = 2.6$ and 8.7 and 10.0 Hz, 1 H), 7.70–7.77 (m, 2 H), 11.93 (br s, 1 H). MS: method A, T_r (min) = 0.65; $[M + H]^+$, m/z 329; $[M - H]^-$, m/z 331.

2-[(7-Fluoro-1,3-benzoxazol-2-yl)methyl]-6-(morpholin-4-yl)pyrimidin-4(3H)-one (32). By a similar procedure to that described for the synthesis of 7 using 500 mg (1.9 mmol) of 2 and 357 mg (2.8 mmol) of 2-amino-6-fluorophenol, 32 (110 mg, 17%) was obtained as a white powder. $^1\text{H NMR}$ (400 MHz): 3.34–3.38 (m, 4 H), 3.53–3.59 (m, 4 H), 4.31 (s, 2 H), 5.26 (s, 1 H), 7.30–7.42 (m, 2 H), 7.59 (dd, $J = 1.4$ and 7.7 Hz, 1 H), 11.93 (br m, 1 H). MS: method B, T_r (min) = 3.11; $[M + H]^+$, m/z 331; $[M - H]^-$, m/z 329.

2-(1,3-Benzoxazol-2-ylmethyl)-3-methyl-6-(morpholin-4-yl)pyrimidin-4(3H)-one (33). By a similar procedure to that described for the synthesis of 7 using 261 mg (0.9 mmol) of 4 and 350 mg (3.2 mmol) of 2-aminophenol, 33 (40 mg, 12%) was obtained as a pale-yellow powder, mp 191 °C. $^1\text{H NMR}$ (400 MHz): 3.26 (m, 4 H), 3.40 (s, 3 H), 3.50 (m, 4 H), 4.60 (s, 2 H), 5.37 (s, 1 H), 7.38 (m, 2 H), 7.72 (m, 2 H). MS: method B, T_r (min) = 3.11; $[M + H]^+$, m/z 327; $[M - H]^-$, m/z 325.

2-[(4-Methyl-1,3-benzoxazol-2-yl)methyl]-6-(morpholin-4-yl)pyrimidin-4(3H)-one (34). By a similar procedure to that described for the synthesis of 7 using 1 g (3.8 mmol) of 2 and 471 mg (3.8 mmol) of 2-amino-3-methylphenol, 34 (286 mg, 23%) was obtained as a beige solid. $^1\text{H NMR}$ (400 MHz): 2.50 (masked s, 3 H), 3.24–3.39 (m partially masked, 4 H), 3.56 (m, 4 H), 4.25 (s, 2 H), 5.25 (br s, 1 H), 7.17 (d, $J = 7.8$ Hz, 1 H), 7.26 (t, $J = 7.8$ Hz, 1 H), 7.49 (d, $J = 7.8$ Hz, 1 H), 11.80 (br m, 1 H). MS: method A, T_r (min) = 0.72; $[M + H]^+$, m/z 327; $[M - H]^-$, m/z 325.

2-[(5-Methyl-1,3-benzoxazol-2-yl)methyl]-6-(morpholin-4-yl)pyrimidin-4(3H)-one (35). By a similar procedure to that described for the synthesis of 7 using 500 mg (1.9 mmol) of 2 and 349 mg (2.8 mmol) of 2-amino-4-methylphenol, 35 (280 mg, 45%) was obtained as a white solid, mp 242 °C. $^1\text{H NMR}$ (400 MHz): 2.41 (s, 3 H), 3.35 (m, 4 H), 3.56 (m, 4 H), 4.22 (s, 2 H), 5.24 (br s, 1 H), 7.19 (dd, $J = 1.9$ and 8.3 Hz, 1 H), 7.51 (d, $J = 1.9$ Hz, 1 H), 7.57 (d, $J = 8.3$ Hz, 1 H), 11.91 (br m, 1 H). MS: method A, T_r (min) = 0.74; $[M + H]^+$, m/z 327; $[M - H]^-$, m/z 325.

2-[(6-Methyl-1,3-benzoxazol-2-yl)methyl]-6-(morpholin-4-yl)pyrimidin-4(3H)-one (36). By a similar procedure to that described for the synthesis of 7 using 400 mg (1.5 mmol) of 2 and 466 mg (3.8 mmol) of 2-amino-5-methylphenol, 36 (105 mg, 21%) was obtained as a white solid. $^1\text{H NMR}$ (400 MHz): 2.43 (s, 3 H), 3.36 (m, 4 H), 3.56 (m, 4 H), 4.21 (s, 2 H), 5.24 (br m, 1 H), 7.18 (br d, $J = 8.3$ Hz, 1 H), 7.51 (br s, 1 H), 7.57 (d, $J = 8.3$ Hz, 1 H), 11.91 (br m, 1 H). MS: method A, T_r (min) = 0.69; $[M + H]^+$, m/z 327; $[M - H]^-$, m/z 325.

2-[(7-Methyl-1,3-benzoxazol-2-yl)methyl]-6-(morpholin-4-yl)pyrimidin-4(3H)-one (37). By a similar procedure to that described for the synthesis of 7 using 1 g (3.8 mmol) of 2 and 680 mg (5.5 mmol) of 2-amino-6-methylphenol, 37 (835 mg, 67%) was obtained as a beige solid. $^1\text{H NMR}$ (400 MHz): 2.47 (s, 3 H), 3.37 (m, 4 H), 3.57 (m, 4 H), 4.25 (s, 2 H), 5.25 (s, 1 H), 7.20 (d, $J = 7.8$ Hz, 1 H), 7.25 (t, $J = 7.8$ Hz, 1 H), 7.52 (d, $J = 7.8$ Hz, 1 H), 11.90 (br s, 1

H). MS: method A, T_r (min) = 0.69; $[M + H]^+$, m/z 327; $[M - H]^-$, m/z 325.

2-[(4-Bromo-1,3-benzoxazol-2-yl)methyl]-6-(morpholin-4-yl)pyrimidin-4(3H)-one (38). By a similar procedure to that described for the synthesis of 7 using 5.0 g (19.1 mmol) of 2 and 3.6 g (19.1 mmol) of 2-amino-3-bromophenol, 38 (1.22 g, 16%) was obtained as a white solid. $^1\text{H NMR}$ (400 MHz): 2.50 (masked s, 3 H), 3.35 (m, 4 H), 3.56 (m, 4 H), 4.31 (s, 2 H), 5.26 (br s, 1 H), 7.35 (t, $J = 8.1$ Hz, 1 H), 7.61 (d, $J = 8.1$ Hz, 1 H), 7.75 (d, $J = 8.1$ Hz, 1 H), 11.94 (br m, 1 H). MS: method A, T_r (min) = 0.70; $[M + H]^+$, m/z 393; $[M - H]^-$, m/z 391.

6-(Morpholin-4-yl)-2-[(4-phenyl-1,3-benzoxazol-2-yl)methyl]pyrimidin-4(3H)-one (39). A mixture of 38 (130 mg, 0.332 mmol), phenylboronic acid (45 mg, 0.4 mmol), Pd(PPh₃)₄ (38 mg, 0.03 mmol), sodium carbonate (83 mg, 0.8 mmol) in water (3 mL), and 1,2-dimethoxyethane (5 mL) was stirred at 100 °C for 5 h and then evaporated to dryness under reduced pressure. Water and dichloromethane were added to the residue, and the organic layer was washed with brine and dried over anhydrous magnesium sulfate. The filtrate was concentrated, and the residue was purified by flash chromatography (dichloromethane/methanol: 95/05) to give 39 (68 mg, 53%) as a white solid. $^1\text{H NMR}$: 3.34 (m, 4 H), 3.55 (m, 4 H), 4.32 (s, 2 H), 5.24 (s, 1 H), 7.41 (t, $J = 7.8$ Hz, 1 H), 7.45–7.54 (m, 3 H), 7.61 (d, $J = 7.8$ Hz, 1 H), 7.70 (d, $J = 7.8$ Hz, 1 H), 7.98 (d, $J = 7.8$ Hz, 2 H), 11.92 (br m, 1 H). MS: method A, T_r (min) = 0.88; $[M + H]^+$, m/z 389; $[M - H]^-$, m/z 387.

6-(Morpholin-4-yl)-2-[(7-phenyl-1,3-benzoxazol-2-yl)methyl]pyrimidin-4(3H)-one (40). By a similar procedure to that described for the synthesis of 7 using 330 mg (1.3 mmol) of 2 and 467 mg (2.5 mmol) of 2-amino-6-phenylphenol, 40 (73 mg, 15%) was obtained as a pale-green solid. $^1\text{H NMR}$ (400 MHz): 3.36 (m, 4 H), 3.54 (m, 4 H), 4.30 (s, 2 H), 5.24 (br s, 1 H), 7.41–7.50 (m, 2 H), 7.55 (t, $J = 7.8$ Hz, 2 H), 7.65 (d, $J = 7.8$ Hz, 1 H), 7.71 (d, $J = 7.8$ Hz, 1 H), 7.88 (d, $J = 7.8$ Hz, 2 H), 11.91 (br m, 1 H). MS: method A, T_r (min) = 0.85; $[M + H]^+$, m/z 389; $[M - H]^-$, m/z 387.

6-(Morpholin-4-yl)-2-[(4-(thiophen-2-yl)-1,3-benzoxazol-2-yl)methyl]pyrimidin-4(3H)-one (41). By a similar procedure to that described for the synthesis of 39 using 200 mg (0.51 mmol) of 38 and 73 mg (0.57 mmol) of thiophene-2-boronic acid, 41 (30 mg, 15%) was obtained as a gray solid. $^1\text{H NMR}$ (400 MHz): 3.20–3.40 (m partially masked, 4 H), 3.55 (m, 4 H), 4.35 (s, 2 H), 5.24 (s, 1 H), 7.21 (dd, $J = 3.7$ and 5.1 Hz, 1 H); 7.42 (t, $J = 7.8$ Hz, 1 H), 7.60–7.71 (m, 3 H), 8.00 (dd, $J = 1.2$ and 3.7 Hz, 1 H), 12.01 (br m, 1 H). MS: method A, T_r (min) = 0.87; $[M + H]^+$, m/z 395; $[M - H]^-$, m/z 393.

6-(Morpholin-4-yl)-2-[(4-(pyridin-2-yl)-1,3-benzoxazol-2-yl)methyl]pyrimidin-4(3H)-one (42). By a similar procedure to that described for the synthesis of 7 using 550 mg (2.1 mmol) of 2 and 460 mg (2.5 mmol) of 2-amino-3-(pyridin-2-yl)phenol (102 mg, 12%), 42 was obtained as pale yellow solid. $^1\text{H NMR}$ (400 MHz): 3.20–3.40 (m, partially masked, 4 H), 3.54 (m, 4 H), 4.37 (s, 2 H), 5.26 (s, 1 H), 7.40 (m, 1 H), 7.52 (t, $J = 7.8$ Hz, 1 H), 7.80 (dd, $J = 1.0$ and 7.8 Hz, 1 H), 7.96 (dt, $J = 2.0$ and 7.8 Hz, 1 H), 8.24 (dd, $J = 1.0$ and 7.8 Hz, 1 H), 8.69 (d, $J = 7.8$ Hz, 1 H), 8.74 (m, 1 H), 11.92 (br m, 1 H). MS: method A, T_r (min) = 0.52; $[M + H]^+$, m/z 390; $[M - H]^-$, m/z 388.

6-(Morpholin-4-yl)-2-[(4-(pyridin-3-yl)-1,3-benzoxazol-2-yl)methyl]pyrimidin-4(3H)-one (43). By a similar procedure to that described for the synthesis of 39 using 130 mg (0.33 mmol) of 38 and 45 mg (0.37 mmol) of pyridine-3-boronic acid, 43 (30 mg, 23%) was obtained as a white solid. $^1\text{H NMR}$ (400 MHz): 3.35 (m, 4 H), 3.55 (m, 4 H), 4.33 (m, 2 H), 5.25 (s, 1 H), 7.50–7.58 (m, 2 H), 7.70 (d, $J = 7.8$ Hz, 1 H), 7.78 (d, $J = 8.1$ Hz, 1 H), 8.36 (td, $J = 2.0$ and 7.8 Hz, 1 H), 8.61 (dd, $J = 1.7$ and 4.9 Hz, 1 H), 9.19 (d, $J = 2.0$ Hz, 1 H), 11.94 (br m, 1 H). MS: method A, T_r (min) = 0.49; $[M + H]^+$, m/z 390; $[M - H]^-$, m/z 388.

6-(Morpholin-4-yl)-2-[(4-(pyridin-4-yl)-1,3-benzoxazol-2-yl)methyl]pyrimidin-4(3H)-one (44). By a similar procedure to that described for the synthesis of 39 using 200 mg (0.51 mmol) of 38 and 115 mg (0.94 mmol) of pyridine-4-boronic acid pinacol ester, 44 (30 mg, 15%) was obtained as a beige solid. $^1\text{H NMR}$ (400 MHz): 3.20–3.40 (m, partially masked, 4 H), 3.54 (m, 4 H), 4.35 (s, 2 H), 5.25 (s, 1

H), 7.54 (t, $J = 7.8$ Hz, 1 H), 7.79 (d, $J = 7.8$ Hz, 1 H), 7.83 (d, $J = 7.8$ Hz, 1 H), 8.04 (d, $J = 5.9$ Hz, 2 H), 8.70 (d, $J = 5.9$ Hz, 2 H), 11.95 (br m, 1 H). MS: method A, T_r (min) = 0.45; $[M + H]^+$, m/z 390; $[M - H]^-$, m/z 388.

2-[(5-Fluoro-4-phenyl-1,3-benzoxazol-2-yl)methyl]-6-(morpholin-4-yl)pyrimidin-4(3H)-one (45). By a similar procedure to that described for the synthesis of 7 using 630 mg (2.4 mmol) of 2 and 445 mg (2.2 mmol) of 2-amino-6-fluorobiphenyl-3-ol (see Scheme 6), (127 mg, 13%), 45 was obtained as a beige solid. 1H NMR (400 MHz): 3.34 (m, 4 H), 3.55 (m, 4 H), 4.29 (s, 2 H), 5.23 (br s, 1 H), 7.38 (dd, $J = 9.0$ and 11.2 Hz, 1 H), 7.45 (t, $J = 7.8$ Hz, 1 H), 7.52 (t, $J = 7.8$ Hz, 2 H), 7.68 (d, $J = 7.8$ Hz, 2 H), 7.76 (dd, $J = 4.0$ and 9.0 Hz, 1 H), 11.94 (br m, 1 H). MS: method A, T_r (min) = 0.88; $[M + H]^+$, m/z 407; $[M - H]^-$, m/z 405.

2-Amino-6-fluorobiphenyl-3-ol. To a suspension of 16 g (84 mmol) of 3-bromo-4-fluorophenol and 16 g of ammonium nickel(II)sulfate hexahydrate (41 mmol) in 100 mL of dichloromethane was added 8.1 g of nitric acid ($d = 1.41$, 89.6 mmol) over 8 min while maintaining the internal temperature below 25 °C with an ice bath. The resulting mixture was allowed to stir for 20 min and poured into 250 g of crushed ice. The layers are separated and the aqueous phase extracted with dichloromethane. The organic layers were combined, washed with brine, dried over anhydrous magnesium sulfate, and then concentrated under reduced pressure. The residue was purified by flash chromatography; eluent, dichloromethane/heptane 70/30 to give 3-bromo-4-fluoro-2-nitrophenol (6.1 g, 31%) as a yellow solid. 1H NMR (300 MHz): 7.11 (dd, $J = 4.3$ and 9.3 Hz, 1 H), 7.46 (dd, $J = 8.5$ and 9.3 Hz, 1 H), 11.41 (br s, 1 H).

A mixture of 5.2 g (22 mmol) of 3-bromo-4-fluoro-2-nitrophenol, 5.5 g (27 mmol) of 4,4,5,5-tetramethyl-2-phenyl-1,3,2-dioxaborolane, 1.16 g (1.6 mmol) of Pd(dppf)Cl₂, 21.5 g (66 mmol) of cesium carbonate, 43 mL of water, and 166 mL of dioxane was stirred at 95 °C for 4 h. After cooling to room temperature, water, and ethyl were added and the insoluble material formed filtered off. The organic layer was washed with brine and dried over anhydrous magnesium sulfate. The filtrate was concentrated under reduced pressure, and the residue was purified by flash chromatography; eluent, dichloromethane/heptane 50/50 then 100% dichloromethane to give 6-fluoro-2-nitrophenyl-3-ol (4.5 g, 88%) as a yellow solid. 1H NMR (300 MHz): 7.10 (dd, $J = 4.4$ and 9.2 Hz, 1 H); 7.29–7.35 (m, 2 H), 7.41 (dd, $J = 9.1$ and 9.2 Hz, 1 H), 7.43–7.50 (m, 3 H), 11.04 (br s, 1 H).

To a solution of 4.4 g (19 mmol) of 6-fluoro-2-nitrophenyl-3-ol in 75 mL of acetic acid, 5.1 g (91 mmol) of iron powder were added. The reaction mixture was stirred at 70 °C during 30 min and then evaporated to dryness under reduced pressure. The residue was taken up in a mixture of water and ethyl acetate. The insoluble material was filtered off and the aqueous layer extracted with ethyl acetate. The organic layers were combined, washed with brine, dried over anhydrous magnesium sulfate, and then concentrated under reduced pressure. The residue was purified by flash chromatography; eluent, heptane/ethyl acetate 80/20 to give 2-amino-6-fluorobiphenyl-3-ol (3.0 g, 78%) as a yellow solid. 1H NMR (300 MHz): 4.19 (br s, 2 H), 6.31 (dd, $J = 8.6$ and 9.5 Hz, 1 H), 6.63 (dd, $J = 5.4$ and 8.6 Hz, 1 H), 7.29–7.50 (m, 5 H), 9.19 (br s, 1 H).

In Vitro PI3K Enzyme Assay. Human p110 α and δ with N-terminal poly-His tags were coexpressed with p85 α in a Sf9 baculovirus expression system, and the p110 α , δ /p85 α heterodimers were purified by sequential Ni-NTA and heparin chromatography. Human p110 β with N-terminal poly-His tag was coexpressed with p85 α in a S21 baculovirus expression system, and the p110 β /p85 α heterodimer was purified by sequential Ni-NTA, A-EX (Q-HP), and Superdex S200 chromatography. A truncated form of human PI3K γ encompassing residues 114–1102, N-terminally labeled with poly-His tag, was expressed with baculovirus in Sf9 insect cells and purified by sequential Ni-NTA, Superdex-200 chromatography. Lipid kinase activity assays were performed using PI3K HTRF (homogeneous time-resolved fluorescence) Millipore Kit in 384-well format according to manufacturer instructions. The assay was performed in 10 μ L reaction volume: serial dilutions of inhibitors (3% DMSO) were preincubated for 15 min at room temperature (RT) with 10 μ M

PI(4,5)P2 substrate/enzyme mixture before starting the reaction by the addition of 100 μ M ATP. Enzyme concentrations corresponded to 100 pM, 15 pM, 30 pM, and 400 pM for α , β , δ , and γ isoforms, respectively. After 15 min of incubation at RT, the reaction was stopped by adding a mixture of PIP3-biotin and stop solution (Millipore Kit). Detection mixture, containing streptavidin-coupled allophycocyanin (SA-XL665) and precombined GST-pleckstrin homology (GST-PH) domain with Anti-GST-europium labeled, was then added. After overnight incubation at 4 °C, HTRF signals were measured with a Rubystar (BMG Labtech). For this competition binding assay, wells without enzyme were used to calculate the maximal signal (max). The nontreated wells containing 3% DMSO were used to determine the minimum signal (min). The percentage inhibition was calculated for each concentration of compound according to the following formula [% inhibition = ((Test – min)/(max – min)) \times 100]. The activity of the product was estimated by using the concentration of compound where percent inhibition is equal to 50 (IC₅₀) obtained from a dose–response curve with 11 increasing concentrations tested in single replicates and fitted with XLfit 4 software from Excel version 4.2.2 using the 4-parameter logistic model (eq 205). IC₅₀ values represent the mean from at least two independent experiments; when more than a 3-fold difference was observed between the two independent values, additional experiments were performed in order to determine the mean IC₅₀.

Akt Phosphorylation Cell-Based Assays. Cell lines were purchased from ATCC.³⁶ Cells were cultured in DMEM medium, containing 10% fetal calf serum and 1% glutamine (complete culture medium).

MEF-3T3-myristoylated p110 β cell line was an inducible stable clone established by transfecting a pTRE2Hygro-myc vector and human myr wt PI3KC β sequence of interest in Mouse Embryonary Fibroblast MEF3T3 Tet Off (Clontech 631139). Cells were cultured in DMEM medium supplemented with 10% tet system approved FCS, 2 mM L-glutamine, 100 μ g/mL geneticin, 200 μ g/mL hygromycin B. MEF-3T3-myristoylated p110 δ cell line was an inducible stable clone established by transfecting a pTRE2Hygro-myc vector and human myr wt PI3KC δ sequence of interest in Mouse Embryonary Fibroblast MEF3T3 Tet Off (Clontech 631139). Cells were cultured in the same medium as described for MEF-3T3-myristoylated p110 β . Akt phosphorylation test was based on a sandwich immunoassay using the MSD Multispot Biomarker Detection kit from Meso Scale Discovery “phospho-Akt (Ser473) whole cell lysate kit” (no. K151CAD). The primary antibody specific for pAkt-S473 was coated onto an electrode in each well of the 96-well plates of the MSD kit. After the addition of a protein lysate to each well, the signal was visualized by adding a secondary detection antibody labeled with an electrochemiluminescent compound. The procedure followed was that described in the MSD kit. On day 1, cells were seeded into 96-well plates at the concentration of 5000–35000 cells/well depending on the cell line (PC3 and H460 cells), 20000 cells/well (MEF-3T3-myristoylated p110 δ and MEF-3T3-myristoylated p110 β cells) or 320000 cells/well (Raw 264.7 cells) in 200 μ L of DMEM complete medium (PC3, MEF-3T3-myristoylated p110 β and MEF-3T3-myristoylated p110 δ cells) or in serum-free medium (Raw 264–7 cells), and incubated at 37 °C, 5% CO₂, overnight. On day 2, cells were incubated in the presence or absence of the test products for 30 min to 2 h at 37 °C in the presence of 5% of CO₂. In the case of Raw 264.7, at the end of compound treatment, cells were stimulated for 5 min with C5a at 10^{–8} M final concentration, at 37 °C in the presence of 5% of CO₂. In the case of MEF-3T3-myristoylated p110 δ , cells were serum-deprived for 6 h before treatment with test compounds in serum-free medium. The test compounds, diluted in DMSO, were added from a 20-time concentrated stock solution, the final DMSO concentration being 0.1%. The compounds were tested at increasing concentrations ranging from less than 1 nM to 10 μ M. After incubation, cells were lysed for the preparation of the proteins, according to the MSD kit description. The plates were read on the S12400 instrument from Meso Scale Discovery. Wells without cells and containing the lysis buffer were used to determine the background noise subtracted from all the measurements (min). The wells

containing cells in the absence of product and in the presence of 0.1% DMSO were used to determine the 100% signal (max). The percentage inhibition was calculated for each concentration of compound according to the following formula [% inhibition = $(1 - (\text{Test} - \text{min})/(\text{max} - \text{min})) \times 100$]. The activity of the product was estimated by using the IC_{50} obtained from a dose–response curve with 10 concentrations tested in triplicate and fitted with XLFit 4 software from Excel version 4.2.2 using the 4-parameter logistic model (eq 205). IC_{50} values represent the mean from at least two independent experiments; when more than a 3-fold difference was observed between the two independent values, additional experiments were performed in order to determine the mean IC_{50} .

The measurement of Akt phosphorylation on threonine 308 residue (pAkt-T308) was evaluated by Western blotting using a primary antibody specific for pAkt-T308. Briefly, on day 1, PC3 cells were seeded into 6-well microplates at 800000 cells per well, in complete culture medium containing 10% FCS and incubated at 37 °C, 5% CO_2 , overnight. On day 2, the cells were incubated in the presence or absence of compound 8 for 30 min to 2 h at 37 °C in the presence of 5% of CO_2 . At the end of cell treatment period, adherent cells were lysed for the preparation of the proteins. Cells were lysed in a lysis buffer containing Hepes 50 mM, NaCl 150 mM, glycerol 10%, Triton X100 1%, pH = 7.5, adding extemporaneously a cocktail of protease and phosphatase inhibitors diluted 100-fold (Roche, Protease and Phosphatase Inhibitor Cocktail, reference 1836153 and 104906837001, respectively). Protein concentrations in each sample were determined using microBCA technique according to manufacturer's instructions (MicroBCA Protein assay kit, Kit Pierce reference 23235). Western blotting was performed loading 20 μ g of proteins in each gel well; pAkt-T308 was revealed using antiphospho Akt Thr308 rabbit monoclonal antibody (Cell Signaling Technology, reference 4056) followed by an antirabbit IgG HRP conjugate antibody (Promega, reference W401B). GAPDH was revealed in control using anti-GAPDH rabbit monoclonal antibody 14C10 (Cell Signaling Technology, reference 2118), followed by the same antirabbit IgG HRP conjugate antibody. After Western blotting revelation according to the operating procedure instructions, luminescence was read using FujiFilm (Ray Test) apparatus. This instrument measures the total signal of luminescence obtained on Fujifilm machine (AU) for each selected band. Then, it subtracts the background value (BG) proportional to the size of the selected band or area. The background is calculated from a band taken on the specific background of the Western blot to obtain the specific signal or (AU-BG) for each band. The software of the machine calculates the percentage of specific activity obtained for each band as a function of a standard signal selected as the 100% (DMSO 0.1%), which gives the percentage of inhibition for each compound concentration. The activity of the product was estimated by using the IC_{50} obtained from a dose–response curve with six concentrations tested in single replicate and fitted with XLFit 4 software from Excel version 4.2.2 using the four-parameter logistic model (eq 205). IC_{50} values represent the mean from at least two independent experiments; when more than a 3-fold difference was observed between the two independent estimations, additional experiments were performed in order to determine the mean IC_{50} .

In Vivo PD Assay. CB17/ICR-Prkdc severe combined immunodeficiency (SCID)/Crl mice, at 6–10 weeks old, were bred at Charles River France (Domaine des Oncins, 69210 L'Arbresle, France) from strains obtained from Charles River, USA, and were over 17 g at start of treatment after an acclimatization time of at least 5 days. All in vivo protocols were approved by local ethical committee. For PK/PD studies, animals bearing tumors were randomized according to a given median tumor burden range on a specific day post tumor implantation, and treatment was administered as indicated with three animals per group. At designated time point post-treatment as indicated, mice were anesthetized and euthanized, and blood samples were collected and kept for PK analysis. Tumors were resected, frozen in dry ice in small fragments in a screw-capped tube containing 2.8 mm ceramic beads (Ozyme BER1030), and stored at –80 °C until use. Protein extracts were prepared in lysis buffer [10 mM Tris pH 7.5 (Invitrogen 15567–

027), 100 mM NaCl (Sigma S5150), 1 mM EDTA pH 8 (Invitrogen 15575–038), 1 mM EGTA pH 8 (Sigma E4378), 1% Triton (Sigma T9284), 1 mM NaF (Sigma S7920), 20 mM Na₄P₂O₇ (Sigma S6422), 1 mM activated Na₃VO₄ (Sigma S6508), 10% glycerol (Fisher Scientific G/0650/17) supplemented with protease inhibitor mix (Roche 11836145001)] by mechanical dissociation using the Precellys 24 bead beating homogenizer (Ozyme, BER1011) set at two runs of 2 × 30 s at 6000 rpm at 4 °C and connected to a Cryolys cooling system. The extracts were incubated 2 h at 4 °C to extract membrane proteins, clarified by a 16000g centrifugation for 15 min at 4 °C, and supernatants were collected, aliquoted, snap-frozen in dry ice, and stored at –80 °C until analysis.

Protein concentrations were determined by the Bradford method (Kit Pierce BCA 23225) according to the manufacturer instructions. Tumors extract samples were not diluted for the assays. Levels of total protein Akt and phospho protein pAkt-S473 and pAkt-T308 were determined using Mesoscale electrochemiluminescence duplex immunoassays according to manufacturer instructions. The impact on biomarker upon compound treatment was expressed as the mean modulation of target kinase phosphorylation in treated tumors as compared to the control (animals treated with vehicle) and was calculated as $[100 - ((\text{mean phospho protein for treated group})/(\text{mean phospho protein for vehicle group})) \times 100]$. Results of percentages of inhibition are reported as the mean and standard error of the mean of three mice per group.

Xenograft Studies. Human prostate PC-3 cells were purchased at ATCC (Batch CTRL-1435, Rockville, MD, USA). The PC-3 was initiated from a bone metastasis of grade V prostatic adenocarcinoma from a 62-year-old male Caucasian. The PC-3 cells were cultured in F-12 medium + 10% fetal calf serum (FCS) + 2 mL glutamin. The tumor model was established by implanting subcutaneously (sc) 3×10^6 cells mixed with 50% matrigel (Reference 356234, Becton Dickinson Biosciences) per SCID female mice and was maintained by sc serial passages once every 3 weeks in SCID female mice. Animals bearing tumors were randomized according to a given median tumor burden range on a specific day post tumor implantation, and the compound was administered orally at 300 mg/kg twice a day (bid) in suspension prepared in 0.6% methylcellulose (MC) and 0.5% Tween 80, with 10 animals per group. Tumor volume was measured regularly during the treatment period.

Changes in tumor volume for each treated (T) and control (C) group were calculated for each tumor by subtracting the tumor volume on the day of first treatment (staging day) from the tumor volume on the specified observation day. The median ΔT was calculated for the treated group, and the median ΔC was calculated for the control group. Then the ratio $\Delta T/\Delta C$ was calculated and expressed as a percentage.

The dose was considered as therapeutically active when $\Delta T/\Delta C$ was lower than 40%.³⁷

For statistical analysis, a two-way ANOVA with repeated measures was applied to the ranks of the tumor volume changes from baseline (TV_{day} – TV₀) and (CV_{day} – CV₀), followed by a Winer analysis at each day of tumor measurement. In case of significance, a Dunnett's test was performed versus vehicle. This statistical analysis was performed on SAS system release 8.2 for SUN4 via Everstat 5.0 software. A probability less than 5% ($p < 0.05$) was considered as significant.³⁷

Crystallography: Determination of p110 δ Crystal Structure. Mouse p110 δ (106–1044) was expressed and purified according to published procedures.²⁷ The protein crystallized in presence of 6–9% (w/v) poly ethylene glycol (PEG) 8000, 12–18% ethylene glycol, 100 mM of a carboxylic acids mixture (sodium formate, sodium citrate, sodium oxamate, ammonium acetate, and potassium/sodium tartrate) in 100 mM MES/imidazole buffer pH 6.5 at 20 °C, and a solution of crystal seeds diluted to 1/200000. Crystal seeds were obtained by crystallizing the protein in presence of 14–16% PEG 8000, 28–32% ethylene glycol, and 100 mM carboxylic acids in 100 mM MES/Imidazole buffer pH 6.5. Co-crystals were obtained by mixing 1 μ L of protein (10 mg/mL), 1 mM compound 8 and 1 μ L of precipitant with 0.2 μ L of the diluted seeding solution. Crystals were flash-frozen in

liquid nitrogen prior to data collection. Diffraction data for p110 δ -compound **8** were collected at the European Synchrotron Radiation Facility, beamline ID29 using $\lambda = 0.9784 \text{ \AA}$ and a Pilatus 6 M detector (DECTRIS Ltd.). Data were processed using autoPROC,³⁸ and the structure was solved by molecular replacement using MOLREP³⁹ with the mouse p110 δ structure as the search model (PDB code 2WXF) (Table 8). The structure was refined using BUSTER/TNT⁴⁰ and model building was performed with COOT.⁴¹ Coordinates and structure factors were deposited at the Protein Data Bank under the code 4AJW.

AUTHOR INFORMATION

Corresponding Author

*Phone: +33(0)1 58 93 36 14. Fax: +33(0)1 58 93 80 14. E-mail: frank.halley@sanofi.com.

Notes

The authors declare no competing financial interest.

ACKNOWLEDGMENTS

We thank Agnès Vergezac, Laurent Bassinet, Virginie Boisrobert, Laurent Dassenecourt, Françoise Hervé, Alexandre Rohaut, Anne Thomas, Yvette Ruffin, Véronique Lalleman, Marie-France Bachelot, Frédéric Foucault, and Chagri Boumaya for their technical assistance. We thank Dr. Carlos Garcia-Echeverria for his guidance and thorough proofreading of the manuscript.

DEDICATION

This paper is dedicated to the memory of our friend and colleague Dominique Damour.

ABBREVIATIONS USED

bid, bis in die (twice a day); DCM, dichloromethane; DIPEA, diisopropylethylamine; DMF, *N,N*-dimethylformamide; DMSO, dimethyl sulfoxide; EC₅₀, effective concentration at half maximal effect; EDCl, 1-ethyl-3-(3-dimethylaminopropyl)-carbodiimide; HLM, human liver microsomes; IC₅₀, inhibitory concentration at half-maximal effect; iv, intravenous; LE, ligand efficiency; PAkt, phosphoserine–threonine kinase Akt; MES, 4-morpholineethanesulfonic acid; PD, pharmacodynamic; PI3K, phosphoinositide 3-kinase; PK, pharmacokinetic; po, per os; PTEN, phosphatase and TENsin homologue; qd, quaque die (once a day); SAR, structure–activity relationship; SBE- β -cyclodextrin, sulfobutyl ether β -cyclodextrin; SCID, severe combined immunodeficiency; TFA, trifluoroacetic acid; THF, tetrahydrofuran; xantphos, 4,5-bis(diphenylphosphino)-9,9-dimethylxanthene

REFERENCES

- (1) Liu, P.; Cheng, H.; Roberts, T. M.; Zhao, J. J. Targeting the phosphoinositide 3-kinase pathway in cancer. *Nature Rev. Drug Discovery* **2009**, *8*, 627–644.
- (2) Zhao, L.; Vogt, P. K. Class 1 PI3K in oncogenic cellular transformation. *Oncogene* **2008**, *27*, 5486–5496.
- (3) Ihle, N. T.; Powis, G. The biological effects of isoform-specific PI3-kinase inhibition. *Curr. Opin. Drug Discovery Dev.* **2010**, *13*, 41–49.
- (4) Ward, S. G.; Finan, P. Isoform-specific phosphoinositide 3-kinase inhibitors as therapeutic agents. *Curr. Opin. Pharmacol.* **2003**, *3*, 426–434.
- (5) Wee, S.; Wiederschain, D.; Maira, S.-M.; Loo, A.; Miller, C.; deBeaumont, R.; Stegmeier, F.; Yao, Y.-M.; Lengauer, C. PTEN-deficient cancers depend on PIK3CB. *Proc. Natl. Acad. Sci. U.S.A.* **2008**, *105*, 13057–1362.

- (6) Jia, S.; Liu, Z.; Zhang, S.; Liu, P.; Zhang, L.; Hyun, S.; Zhang, L. J.; Signoretti, S.; Loda, M.; Roberts, T. M.; Zhao, J. J. Essential roles of PI(3)K–p110 β in cell growth, metabolism and tumorigenesis. *Nature* **2008**, *45*, 776–779.

- (7) Lannutti, B. J.; Meadows, S. A.; Herman, S. E.; Kashishian, A.; Steiner, B.; Johnson, A. J.; Byrd, J. C.; Tyner, J. W.; Loriaux, M. M.; Deininger, M.; Druker, B. J.; Puri, K. D.; Ulrich, R. G.; Giese, N. A. CAL-101, a p110 δ selective phosphatidylinositol-3-kinase inhibitor for the treatment of B-cell malignancies, inhibits PI3K signaling and cellular viability. *Blood* **2011**, *117*, 561–594.

- (8) Herman, S. E.; Gordon, A. L.; Wagner, A. J.; Heerema, N. A.; Zhao, W.; Flynn, J. M.; Jones, J.; Andritsos, L.; Puri, K. D.; Lannutti, B. J.; Giese, N. A.; Zhang, X.; Wei, L.; Byrd, J. C.; Johnson, A. J. Phosphatidylinositol 3-kinase- δ inhibitor CAL-101 shows promising preclinical activity in chronic lymphocytic leukemia by antagonizing intrinsic and extrinsic cellular survival signals. *Blood* **2010**, *116*, 2078–88.

- (9) Jessen, K.; Kessler, L.; Kucharski, J.; Guo, X.; Staunton, J.; Janes, M.; Elia, M.; Banerjee, U.; Lan, L.; Wang, S.; Stewart, J.; Luzader, A.; Darjania, L.; Li, L.; Chan, K.; Martin, M.; Ren, P.; Rommel, C.; Liu, Y. A Potent and Selective PI3K α Inhibitor, INK1117, Targets Human Cancers Harboring Oncogenic PI3KCA Mutations. AACR Special Conference on Targeting PI3K/mTOR Signaling in Cancer, San Francisco, CA, February 24–27, 2011, Poster A171.

- (10) Arteaga C. L. Mechanistic basis for treatment combinations with PI3K inhibitors. 23rd EORTC-NCI-AACR Symposium on Molecular Targets and Cancer Therapeutics, San Francisco, CA, November 12–16, 2011, Abstract CN03–01.

- (11) Markby, D.; Rice, K.; Bussenius, J.; Jaeger, C.; Nguyen, L.; Virone-Oddos, A.; Foster, P. Characterization of Novel Series of Selective PI3K α and PI3K α /mTOR-dual inhibitors. 22nd EORTC-NCI-AACR Symposium on Molecular Targets and Cancer Therapeutics, Berlin, Germany, November 16–19, 2010, Poster 149.

- (12) Virone-Oddos, A.; Halley, F.; Delorme, C.; Bonnevaux, H.; Nicolas, J.-P.; Karlsson, A.; Abecassis, P.-Y.; Vincent, L.; Lengauer, C. Discovery and characterization of PI3K β isoform-selective inhibitors. 22nd EORTC-NCI-AACR Symposium on Molecular Targets and Cancer Therapeutics, Berlin, Germany, November 16–19, 2010, Poster 115.

- (13) Carry, J.-C.; Certal, V.; Halley, F.; Karlsson, K. A.; Schio, L.; Thompson, F. Novel [4-(morpholin-4-yl)-6-oxo-1,6-dihydropyrimidin-2-yl]amide derivatives, their preparation, their pharmaceutical compositions and their use as AKT(PKB) phosphorylation inhibitors for treating cancers. PCT Int. Appl. WO2011001114, 2011.

- (14) Certal, V.; Halley, F.; Virone-Oddos, A.; Delorme, C.; Karlsson, K. A.; Thompson, F.; Filoche-Rommé, B.; El-Ahmad, Y.; Carry, J.-C.; Abecassis, P.-Y.; Bonnevaux, H.; Nicolas, J.-P.; Morales, R.; Michot, N.; Vade, I.; Louboutin, A.; Perron, S.; Doerflinger, G.; Tric, B.; Monget, S.; Schio, L. Preparation and optimization of new 4-(morpholin-4-yl)- (6-oxo-1,6-dihydropyrimidin-2-yl)amide derivatives as PI3K β inhibitors. *Bioorg. Med. Chem. Lett.* to be submitted for publication.

- (15) Certal, V.; Filoche-Romme, B.; Halley, F.; Karlsson, K. A.; Thompson, F. Novel 6-(morpholin-4-yl)pyrimidin-4-(3H)-one derivatives, their preparation, their pharmaceutical compositions and their use as AKT(PKB) phosphorylation inhibitors for treating cancers. PCT Int. Appl. WO2011001115, 2011.

- (16) Hopkins, A. L.; Groom, C. R.; Alex, A. Ligand efficiency: a useful metric for lead selection. *Drug Discovery Today* **2004**, *9*, 430–431.

- (17) Robertson, A. D.; Jackson, S.; Kenche, V.; Yaip, C.; Prabakaran, H.; Thompson, P. Therapeutic preparation and formulation of morpholino-substituted heterocycles as phosphoinositide 3-kinase inhibitors for therapeutic use. PCT Int. Appl. WO200153266, 2001.

- (18) Jackson, S.; Robertson, A. D.; Kenche, V.; Thompson, P.; Prabakaran, H.; Anderson, K.; Abbott, B.; Goncalves, I.; Nesbitt, W.; Schoenwaelder, S. Preparation of morpholinyl- and pyridinyl-substituted heterobicyclic ketones as selective inhibitors of phospho-

nositide 3-kinase β for use against thrombosis. PCT Int. Appl. WO2004016607, 2004.

(19) Walker, E. H.; Pacold, M. E.; Perisic, O.; Stephens, L.; Hawkins, P. T.; Wymann, M. P.; Williams, R. L. Structural Determinants of Phosphoinositide 3-Kinase Inhibition by Wortmannin, LY294002, Quercetin, Myricetin, and Staurosporine. *Mol. Cell* **2000**, *6*, 909–919.

(20) Knight, Z. S.; Gonzalez, B.; Feldman, M. E.; Zunder, E. R.; Goldenberg, D. D.; Williams, O.; Loewith, R.; Stokoe, D.; Balla, A.; Toth, B.; Balla, T.; Weiss, W. A.; Williams, R. L.; Shokat, K. M. A Pharmacological Map of the PI3-K Family Defines a Role for p110 α in Insulin Signaling. *Cell* **2006**, *125*, 733–747.

(21) Guertin, D. A.; Sabatini, D. M. Defining the Role of mTOR in Cancer. *Cancer Cell* **2007**, *12*, 9–22.

(22) Bissantz, C.; Kuhn, B.; Stahl, M. A Medicinal Chemist's Guide to Molecular Interactions. *J. Med. Chem.* **2010**, *53*, 5061–5084.

(23) Battle, G. M.; Allen, F. H. Learning about Intermolecular Interactions from the Cambridge Structural Database. *J. Chem. Educ.* **2012**, *89*, 38–44.

(24) Equilibrated Solubility Protocol: 1 mg of solid was mixed with 500 μ L of 50 mM phosphate buffer at pH7.4 and the suspension was set on a bottle roller at 60 rpm for 16 h at ambient temperature. The mixture was then filtered and the solution analyzed by HPLC for quantization.

(25) Caroa, I.; Boulenc, X.; Roussetb, M.; Meuniera, V.; Bourri a, M.; Juliana, B.; Joyeux, H.; Roquesa, C.; Bergera, Y.; Zweibaumb, A.; Fabre, G. Characterisation of a newly isolated Caco-2 clone (TC-7), as a model of transport processes and biotransformation of drugs. *Int. J. Pharm.* **1995**, *116*, 147–158.

(26) Caliper-based assay on 192 kinases: 79 RTK, 3 STK, 11 STE, 6 CKI, 29 AGC, 37 CAMK, 20 CGMC, 7 Atypical. After a preincubation time of 15 min between the enzyme and the inhibitor, the enzymatic incubations were performed at 28 °C during 90 min in a phosphate buffer at pH 7.4 containing 1 mM DTT, then stopped by EDTA addition. Compound 8 was tested over 3 concentrations (0.1, 1, and 10 μ M).

(27) Berndt, A.; Miller, S.; Williams, O.; Le, D. D.; Houseman, B. T.; Pacold, J. I.; Gorrec, F.; Hon, W.-C.; Ren, P.; Rommel, C.; Gaillard, P.; R ckle, T.; Schwartz, K. M.; Shokat, K. M.; Shaw, J. P.; Williams, R. L. The p110 δ structure: mechanisms for selectivity and potency of new PI(3)K inhibitors. *Nature Chem. Biol.* **2010**, *6*, 117–124.

(28) Knight, Z. S.; Chiang, G. G.; Alaimo, P. J.; Kenski, D. M.; Ho, C. B.; Coan, K.; Abraham, R. T.; Shokat, K. M. Isoform-specific phosphoinositide 3-kinase inhibitors from an arylmorpholine scaffold. *Bioorg. Med. Chem. Lett.* **2004**, *12*, 4749–4759.

(29) Alaimo, P. J.; Knight, Z. A.; Shokat, K. M. Targeting the gatekeeper residue in phosphoinositide 3-kinases. *Bioorg. Med. Chem.* **2005**, *13*, 2825–2836.

(30) Zhang, X.; Vadas, O.; Perisic, O.; Anderson, K. E.; Clark, J.; Hawkins, P. T.; Stephens, L. R.; Williams, G. L. Structure of Lipid Kinase p110b/p85b Elucidates an Unusual SH2-Domain-Mediated Inhibitory Mechanism. *Mol. Cell* **2011**, *41*, 567–578.

(31) Meyer, H.; Bossert, F.; Horstmann, H. Dihydropyridines, III. Synthesis of 2-aminodihydropyridines via Michael addition. *Liebigs Ann. Chem.* **1977**, *11–12*, 1895–1908.

(32) Cocco, M. T.; Congiu, C.; Maccioni, A.; Plumitallo, A.; Schivo, M. L.; Palmieri, G. Synthesis and biological activity of some pyrrole derivatives. *Farmaco, Ed. Sci.* **1988**, *43*, 103–12.

(33) Lal, B.; D'Sa, A. S.; Kulkarni, B. K.; De Souza, N. J. A convenient one-pot entry into novel 2-substituted-6,7-dihydro-4H-pyrimido[2,1-a]isoquinolin-4-ones. *Tetrahedron* **1990**, *46*, 1323–1330.

(34) Kantlehner, W. Product subclass 17: 1,1-Bis(nitrogen-functionalized) alk-1-enes: alk-1-ene-1,1-diamines. *Sci. Synth.* **2006**, *24*, 571–705.

(35) Landwehr, J.; George, S.; Karg, E.-M.; Poeckel, D.; Steinhilber, D.; Troschuetz, R.; Werz, O. Design and Synthesis of Novel 2-Amino-5-hydroxyindole Derivatives That Inhibit Human 5-Lipoxygenase. *J. Med. Chem.* **2006**, *49*, 4327–4332.

(36) About the ATCC–LGC Standards Partnership; LGC Standards: Teddington, UK; <http://lgcstandards-atcc.org/>.

(37) Plowman, J.; Dykes, D. J.; Hollingshead, M.; Simpson-Herren, L.; Alley, M. C. Human tumor xenograft models in NCI drug development in Anticancer Drug Development Guide: Preclinical Screening, Clinical Trials, and Approval. Humana Press Inc.: Totowa, NJ, 1997; pp101–125.

(38) Vonnrhein, C.; Flensburg, C.; Keller, P.; Sharff, A.; Smart, O.; Paciorek, W.; Womack, T.; Bricogne, G. Data processing and analysis with the autoPROC toolbox. *Acta Crystallogr., Sect. D: Biol. Crystallogr.* **2011**, *67*, 293–302.

(39) Collaborative Computational Project, No. 4. The CCP4 suite: programs for protein crystallography. *Acta Crystallogr., Sect. D: Biol. Crystallogr.* **1994**, *50*, 760–3.

(40) Bricogne, G. Ab initio macromolecular phasing: blueprint for an expert system based on structure factor statistics with built-in stereochemistry. *Methods Enzymol.* **1997**, *277*, 14–18.

(41) Emsley, P.; Cowtan, K. Coot: Model-Building Tools for Molecular Graphics. *Acta Crystallogr., Sect. D: Biol. Crystallogr.* **2004**, *12* (Part 1), 2126–2132.